Figure 4. (A) Results of RT/real-time PCR analysis for *PTOVI* in human aortas. Bands for PCR products were detected as specific single bands (246 bp for *AR*, 250 bp for *PTOVI*, and 307bp for *GAPDH*). The amplified products were run on a 2% agarose gel stained with ethidium bromide. Representative photographs for these RT/real-time PCR gene products are illustrated. A = aorta from a 38-year-old man with mild atherosclerotic change; B = aorta from a 72-year-old man with severe atherosclerotic change; C = aorta from a 45-year-old woman with mild atherosclerotic change; D = aorta from a 76-year-old post-menopausal woman with severe atherosclerotic change; P = positive controls; N = negative controls. (B) Results for *PTOVI* mRNA expression levels (*p < 0.05). (C) Results for *AR* mRNA expression levels (*p < 0.05)

degree of atherosclerosis (group B) and in female aorta with a severe degree of atherosclerosis (group D) (p < 0.05) (Figure 4C).

Immunohistochemistry for PTOVI in human aorta

PTOVI protein was expressed in both the nucleus and the cytoplasm of VSMCs in each group examined (Figures 5 and 6). AR protein was expressed in the nuclei of VSMCs in each group (Figures 5 and 6). However, none of the LCA- or PG-M1-positive cells demonstrated any PTOVI immunoreactivity (Figure 5). The relative levels of PTOVI immunoreactivity in the nuclei of neointimal VSMCs were significantly higher in male aorta with a mild degree of atherosclerotic change (group A) than in those of the other groups examined (groups B, C, and D) (Figure 6A). In addition, AR-positive cells in the neointima were also significantly more abundant in male aorta with a mild degree of atherosclerotic changes (group A) than in those of the other groups (groups B, C, and D) (p < 0.05) (Figure 6E). There was also a significant positive correlation between AR and PTOVI immunoreactivity in the nuclei of VSMCs in the neointima (p < 0.05) (data not shown). AR-positive cells in the tunica media were significantly more abundant in male aorta with a mild degree of atherosclerotic change (group A) than in male aorta with a severe degree of atherosclerosis (group B) and in female aorta with a mild degree of atherosclerosis (group C) (p < 0.05) (Figure 6F). However, there

were no significant differences in PTOVI immunoreactivity in the cytoplasm of cells in the neointima or in the nucleus and/or cytoplasm of cells in the tunica media among these groups (Figure 6B, C, and D).

Discussion

In our present study, results of both microarray and quantitative RT-PCR analyses all indicated that *PTOVI* is one of the genes induced by testosterone via AR-dependent pathways in cultured human VSMCs. In addition, siRNA analysis demonstrated that *PTOVI* is involved in AR-mediated VSMC proliferation. Results of both quantitative RT-PCR and immunohistochemical studies in human aorta obtained at autopsy further demonstrated that PTOV1, as well as AR, detected in the nuclei of neointimal VSMCs was abundant in relatively young male aorta at an early stage of atherosclerosis.

PTOVI has been known to be involved in stimulation of cell proliferation [14,15,17]. This gene is a mitogenic factor that shuttles between nucleus and cytoplasm in a cell cycle-dependent manner in prostate carcinoma cells [14,15,17]. In addition, *PTOVI* overexpression induced cell proliferation and facilitated entry of prostate carcinoma cells into the S phase [14,15,17]. Therefore, these findings all indicated that *PTOVI* may play a very important role in the proliferation of VSMCs. However, it is also true that other atherogenic effects on human VSMCs, such as promotion of PDGF-induced VSMC proliferation,
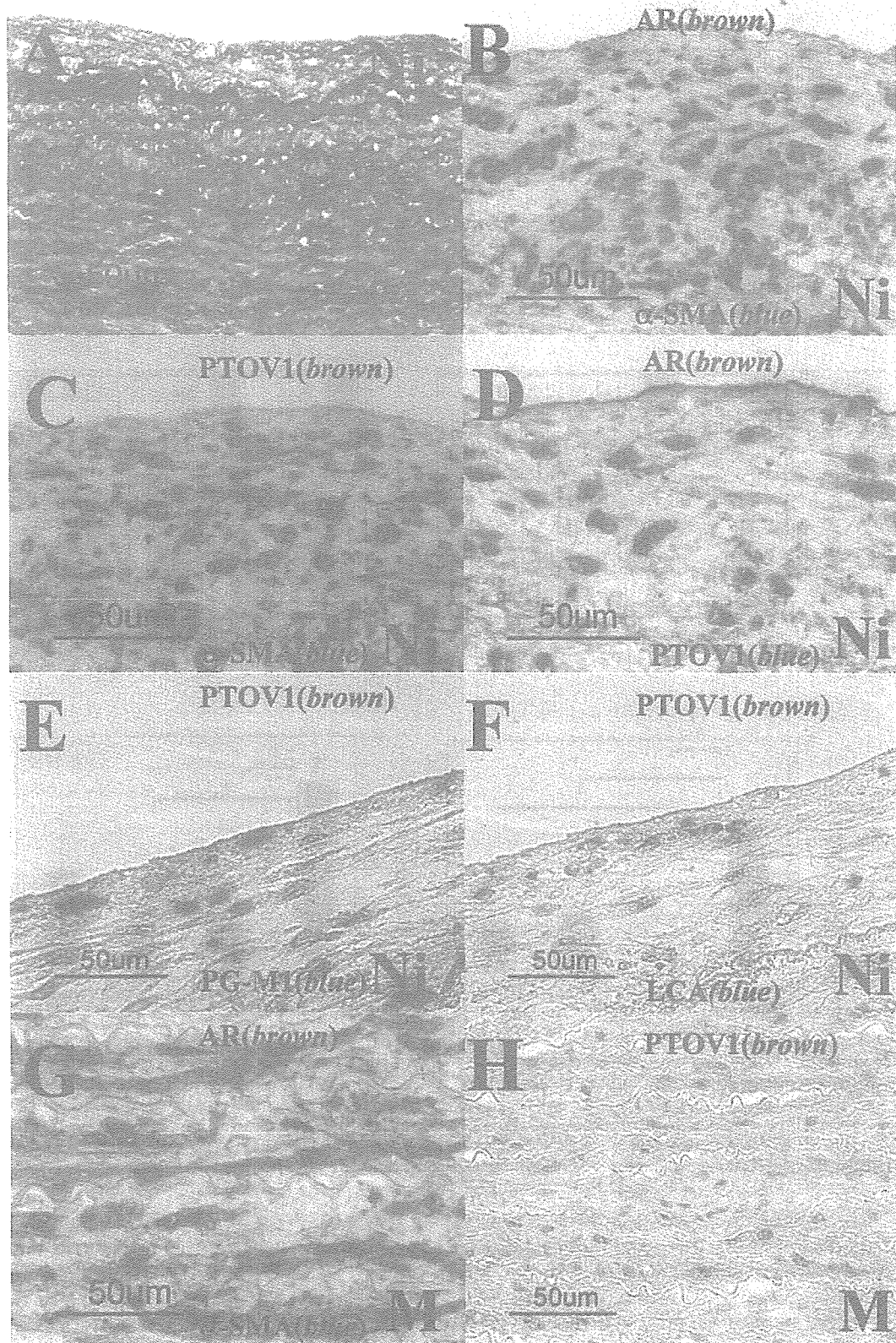
Figure 5. Modified Masson Goldner's stains (A), double-immunohistochemical staining for AR and α-muscle actin (α-SMA) (B), for PTOV1 and α-SMA (C), for AR and PTOV1 (D), for PTOV1 and PG-M1 (E), for PTOV1 and leukocyte common antigen (LCA) (F) in the neointima, double-immunohistochemical staining for AR and α-SMA (G) and immunohistochemical staining for PTOV1 (H) in the media of an abdominal aorta specimen obtained from a 38-year-old man with a mild degree of atherosclerosis (group A). Immunopositive cells appear brown as a result of DAB colorimetric reaction and blue as a result of Vector Blue colorimetric reaction. Double-immunopositive cells are confirmed. Ni = neointima; M = media
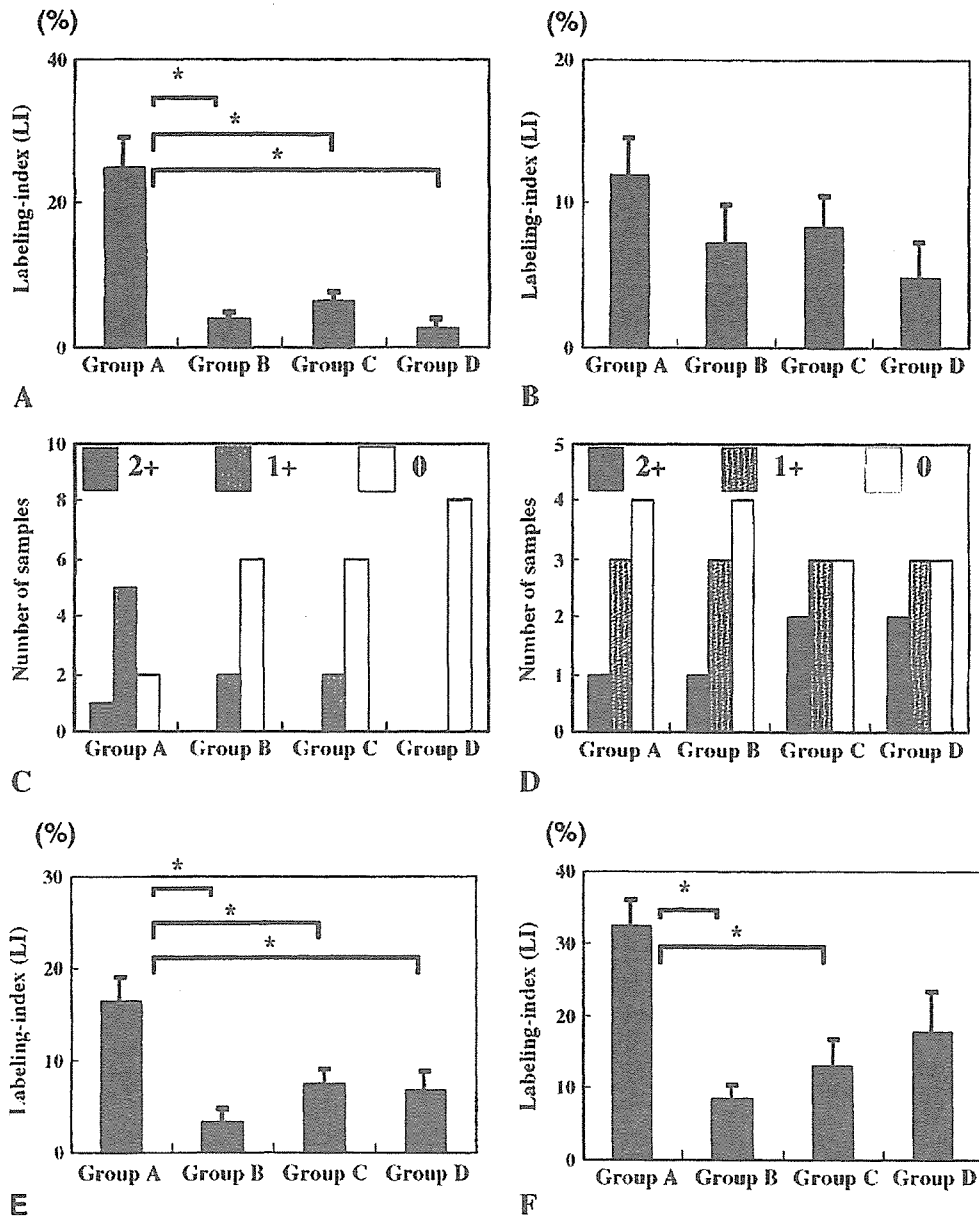
Figure 6. (A, B) The relative immunoreactivity of PTOVI in the nuclei of VSMCs in the neointima (A) and media (B) was evaluated by the labelling index (LI) in each group (0-100), respectively. Data are the mean ± SEM. *p < 0.05, a significant difference between two groups. (C, D) The relative immunoreactivity of PTOVI in the cytoplasm of VSMCs in the neointima (C) and media (D) was evaluated by the percentage of positive cells (0, 1+, and 2+) in each group, respectively. (E, F) The relative immunoreactivity of AR present in the nuclei of VSMCs in the neointima (E) and media (F) was evaluated by the LI in each group (0-100), respectively. Data are the mean ± SEM. *p < 0.05, a significant difference between two groups

have been reported as the mechanism for androgen-induced effects [19,20]. Therefore, further investigations are required to clarify how these pathways interact in exerting androgenic effects on VSMC proliferation in the human vascular system. Our present siRNA study demonstrated that PTOVI may be involved in testosterone-induced VSMC proliferation. However, further investigation is required to clarify the correlation between PTOVI expression and testosterone-induced VSMC proliferation by reconstituting PTOVI expression after transfection of PTOVI siRNA.

Quantitative RT-PCR analysis in our present study also demonstrated that flutamide, an AR-blocker, suppressed androgen-induced PTOVI mRNA expression. The chromosomal region where PTOVI is located, 19q13.3-13.4, has also been demonstrated to harbour a large number of genes whose expression is modulated by androgens [14]. In addition, the expression of PTOVI was reported to be induced by exposure to androgens in LNCaP, an androgen-dependent prostate carcinoma cell line [14,17]. Therefore, these findings all indicate that PTOVI should also be considered one of the testosterone-induced genes in AR-positive VSMCs.

We also demonstrated that PTOV1 immunoreactivity in the nuclei of neointimal VSMCs was abundant in relatively young male aorta associated with early stage atherosclerosis. High levels and nuclear localization of PTOV1 have also been associated with cell proliferation in prostate carcinoma cells [14,17]. Neointimal VSMCs are, therefore, considered to play very important roles in the development of atherosclerosis in humans, particularly at an early stage, compared with VSMCs in the tunica media [10,11]. Therefore, higher expression of PTOV1 in these VSMCs is possibly related to the development of atherosclerosis. Levels of PTOV1 and AR were higher in male aorta with mild atherosclerosis than in female aorta with mild atherosclerosis. Men are generally considered to have a higher risk of developing cardiovascular disease than similarly aged women because of prolonged exposure to higher androgen concentrations [19,21]. It has also been shown recently that androgens upregulate atherosclerosis-related genes in macrophages from men, but not from women, which reflects the complexity of gender-related atherogenesis [19,22].

Our present study also demonstrated that the relative abundance of AR and PTOV1 in neointimal VSMCs was significantly higher in younger male aorta with mild atherosclerotic changes than in male aorta with severe atherosclerotic changes. However, these findings appear to contradict the hypothesis that, if PTOV1 is induced by androgens and implicated in androgenic effects on atherosclerosis, its expression should be higher in male aorta with more severe atherosclerosis than in male aorta with mild atherosclerosis owing to a longer exposure to elevated serum testosterone levels. There are two possible reasons for this: firstly, decreased AR and PTOV1 expression in the neointima of male aorta with severe atherosclerosis may be induced by the age-related decrease in serum testosterone levels [23]; and, secondly, when neointimal formation progresses, VSMCs with AR expression become less abundant than those without AR and these cells are therefore not necessarily influenced by androgenic atherogenic effects. Therefore, PTOV1 expression in the neointimal VSMCs in the aortas of men with high serum androgens levels may be associated with the androgen-induced onset of atherosclerosis; this may be important for formation of the neointima in the early stages of atherogenesis in the male aorta. However, recently, low concentrations of testosterone have been associated with an increased risk of cardiovascular disease in men [24]. Androgens are also known to be a coronary vasodilator, and a study of postmenopausal women demonstrated that endogenous androgens correlated inversely with carotid neointimal thickness, which suggests that androgens have potential beneficial effects on the human vascular system [19,25,26]. These different effects of androgens may depend on differences in the androgen-responsive genes induced, but further investigations are required to clarify possible direct androgenic effects on the human cardiovascular system.

In summary, PTOV1 is considered to be one of the testosterone-induced genes involved in AR-mediated stimulation of VSMC proliferation in the aortic neointima and may play important roles in androgen-related atherogenesis in the male human aorta.

Acknowledgements

References

1. Wingard DL, Suarez L, Barrett-Connor E. The sex differential in mortality from all causes and ischemic heart disease. Am J Epidemiol 1983;117:165–172.
2. Lerner DJ, Kannel WM. Patterns of coronary heart disease morbidity and mortality in the sexes: a 26-year follow-up of the Framingham Study. Am Heart J 1986;111:383–390.
3. McCrohon JA, Jessup W, Handelsman DJ, Celermajer DS. Androgen exposure increases human monocyte adhesion to vascular endothelium and endothelial cell expression of vascular cell adhesion molecule-1. Circulation 1999;99:2317–2322.
4. McCrohon JA, Death AK, Nakhla S, Jessup W, Handelsman DJ, Stanley KK, et al. Androgen receptor expression is greater in macrophages from male than from female donors. A sex difference with implications for atherogenesis. Circulation 2000;101:224–226.
5. Jones RD, Hugh Jones T Channer KS. The influence of testosterone upon vascular reactivity. Eur J Endocrinol 2004;151:29–37.
6. Adams MR, Williams JK, Kaplan JR. Effects of androgens on coronary artery atherosclerosis and atherosclerosis-related impairment of vascular responsiveness. Arterioscler Thromb Vasc Biol 1995;15:562–570.
7. McCrohon JA, Jessup W, Handelsman DJ, Celermajer DS. Androgen exposure increases human monocyte adhesion to vascular endothelium and endothelial cell expression of vascular cell adhesion molecule-1. Circulation 1999;99:2317–2322.
8. Herman SM, Robinson JTC, McCredie RJ, Adams MR, Boyer MJ, Celermajer DS. Androgen deprivation is associated with enhanced endothelium-dependent dilatation in adult men. Arterioscler Thromb Vasc Biol 1997;17:2004–2009.
9. Liu PY, Death AK, Handelsman DJ. Androgens and cardiovascular disease. Endocr Rev 2003;24:313–340.
10. Nakamura Y, Igarashi K, Suzuki T, Kanno J, Inoue T, Tazawa C, et al. E4F1, a novel estrogen-responsive gene in possible atheroprotection, revealed by microarray analysis. Am J Pathol 2004;165:2019–2031.
11. Nakamura Y, Suzuki T, Miki Y, Tazawa C, Senzaki K, Moriya T, et al. Estrogen receptors in atherosclerotic human aorta: inhibition of human vascular smooth muscle cell proliferation by estrogens. Mol Cell Endocrinol 2004;219:17–26.
12. Kondo E, Horii A, Fukushige S. The human PMS2L proteins do not interact with hMLH1, a major DNA mismatch repair protein. J Biochem (Tokyo) 1999;125:818–825.
13. Jaffe IZ, Mendelsohn ME. Angiotensin II and Aldosterone regulate gene transcription via functional mineralocorticoid receptors in human coronary artery smooth muscle cells. Circ Res 2005;96:643–650.
14. Benedit P, Paciucci R, Thomson TM, Valeri M, Nadal M, Caceres C, et al. PTOV1, a novel protein overexpressed in prostate cancer containing a new class of protein homology blocks. Oncogene 2001;20:1455–1464.
15. Santamaria A, Castellanos E, Gomez V, Benedit P, Renau-Piqueras J, Morote J, et al. PTOV1 enables the nuclear

translocation and mitogenic activity of flotillin-1, a major protein of lipid rafts. *Mol Cell Biol* 2005;25:1900–1911.

16. Soslow RA, Dannenberg AJ, Rush D, Woerner BM, Khan KN, Masferrer J, *et al.* COX-2 is expressed in human pulmonary, colonic, and mammary tumors. *Cancer* 2000;89:2637–2645.

17. Santamaria A, Fernandez PL, Farre X, Benedit P, Reventos J, Morote J, *et al.* PTOV-1, a novel protein overexpressed in prostate cancer, shuttles between the cytoplasm and the nucleus and promotes entry into the S phase of the cell division cycle. *Am J Pathol* 2003;162:897–905.

18. Koike G, Winer ES, Horiuchi M, Brown DM, Szpirer C, Dzau VJ, *et al.* Cloning, characterization, and genetic mapping of the rat type 2 angiotensin II receptor gene. *Hypertension* 1995;26:998–1002.

19. Hashimura K, Sudhir K, Nigro J, Ling S, Williams MR, Komesaroff PA, *et al.* Androgens stimulate human vascular smooth muscle cell proteoglycan biosynthesis and increase lipoprotein binding. *Endocrinology* 2005;146:2085–2090.

20. Williams MR, Ling S, Dawood T, Hashimura K, Dai A, Li H, *et al.* Dehydroepiandrosterone inhibits human vascular smooth muscle cell proliferation independent of ARs and ERs. *J Clin Endocrinol Metab* 2002;87:176–181.

21. Gorodeski G, Utian W. Epidemiology and risk factors of cardiovascular disease in postmenopausal women. In *Treatment of the Postmenopausal Woman: Basic and Clinical Aspects*, Lobo R (ed). Raven Press: New York, 1994; 199–221.

22. Ng MK, Quinn CM, McCrohon JA, Nakhla S, Jessup W, Handelsman DJ, *et al.* Androgens up-regulate atherosclerosis-related genes in macrophages from males but not females: molecular insights into gender differences in atherosclerosis. *J Am Coll Cardiol* 2003;42:1306–1313.

23. Snyder PJ, Peachey H, Hannoush P, Berlin JA, Loh L, Lenrow DA, *et al.* Effect of testosterone treatment on body composition and muscle strength in men over 65 years of age. *J Clin Endocrinol Metab* 1999;84:2647–2653.

24. Fukui M, Kitagawa Y, Nakamura N, Kadono M, Mogami S, Hirata C, *et al.* Association between serum testosterone concentration and carotid atherosclerosis in men with type 2 diabetes. *Diabetes Care* 2003;26:1869–1873.

25. Chou TM, Sudhir K, Hutchison SJ, Ko E, Amidon TM, Collins P, *et al.* Testosterone induces dilation of canine coronary conductance and resistance arteries in vivo. *Circulation* 1996;94:2614–2619.

26. Bernini GP, Moretti A, Sgro M, Argenio GF, Barlascini CO, Cristofani R, *et al.* Influence of endogenous androgens on carotid wall in postmenopausal women. *Menopause* 2001;8:43–50.

RESEARCH ARTICLE

Mesp1-Nonexpressing Cells Contribute to the Ventricular Cardiac Conduction System[†]

Satoshi Kitajima,[1*] Sachiko Miyagawa-Tomita,[2] Tohru Inoue,[3] Jun Kanno,[1] and Yumiko Saga[4*]

Previous fate mapping analysis, using Cre recombinase driven by the *Mesp1* locus, revealed that *Mesp1* is expressed in almost all of the precursors of the cardiovascular system, including the endothelium, endocardium, myocardium, and epicardium. *Mesp1*-nonexpressing cells were found to be restricted to the outflow tract cushion and along the interventricular septum (IVS), which is a location that is suggestive of specialized cardiac conduction system (CCS). In our current study, we examined the identity of these IVS cells by using the pattern of β-galactosidase activity in CCS-*lacZ* mice. In addition, by crossing *Mesp1-Cre* and *floxed GFP reporter* mice with CCS-*lacZ* mice, we have calculated that approximately 20% of the ventricular CCS within the IVS corresponds to *Mesp1*-nonexpressing cells. These data suggest that the ventricular CCS is of heterocellular origin. Furthermore, we indicate a possibility that a population of the cells that contribute to the ventricular CCS might be distinguished at an early stage of development. *Developmental Dynamics 235:395–402, 2006.* © 2005 Wiley-Liss, Inc.

Key words: *Mesp1*; mesoderm; heart differentiation; cardiac conduction system; cell-lineage analysis

Accepted 30 September 2005

INTRODUCTION

The heart is the first functional organ to be formed during organogenesis, and cells that are destined to form cardiac mesoderm are induced both before and during gastrulation. The cells of the cardiac mesoderm invaginate through the primitive streak and migrate with the cranial mesoderm. The bilaterally symmetric cardiac precursors subsequently migrate and converge at the midline of the embryo to form the cardiac crescent, which then forms a linear, single heart tube. The heart tube, formed by an outer myocardium and an inner endocardium, then undergoes rightward looping, which is lined by an acellular matrix (the cardiac jelly). The looped heart tube then undergoes septation to generate a mature, four-chambered cardiac structure in mammals.

The heart is composed of three major cardiac cell types: (1) the endocardium, a part of which forms the cushion tissue by transformation from epithelial to mesenchymal cells; (2) the myocardium; and (3) the epicardium (for review, see Moorman and Christoffels, 2003). The major components of the heart, such as endocardium and myocardium, are of mesodermal origin (i.e., cardiogenic mesoderm), but the contribution of other cell lineages has also been reported for both chick and mouse. Fate mapping of the avian cardiac neural crest has been well documented, and it was reported previously from such

experiments using quail–chick chimera that two types of mesenchyme, cardiac neural crest derived and non-neural crest derived, participate in outflow septation and remodeling (Kirby et al., 1983; Waldo et al., 1998). Recently, through the use of the Cre-*loxP* system in mice, it has been demonstrated clearly that the cardiac outflow tract (OT) cushions are contributed in part by cardiac neural crest cells (Yamauchi et al., 1999; Jiang et al., 2000). Additionally, lineage analysis using *Tie2-cre* in mice has suggested that the OT cushions are of mixed origins, containing neural crest cells and endocardium, whereas the atrioventricular (AV) cushions are mainly derived from cells originating from endocardium (Kisanuki et al., 2001).

The specialized cardiac conduction system (CCS) includes the sinoatrial (SA) node, which generates a pacemaker impulse; the AV node, which delays the electrical impulse and allows for the sequential contraction of the atrial and ventricular chambers of the heart; and the ventricular CCS, such as the atrioventricular bundle (AVB), bundle branches, and their ramifications, which facilitates the fast and coordinated conduction of impulses to and throughout the ventricles. Cells in the CCS are characterized by their larger size, reduced number of myofibrils, and large accumulations of glycogen (Mikawa, 1999). It has also been suggested that the CCS might be categorized into two parts based on their origin (Moorman et al., 1998, 2003). One is the SA and AV nodes, which might be derived from the slow-conducting myocardium of the inflow tract and AV canal. The other one is the ventricular CCS, which possibly develops from the trabecular ventricular component. In chick, an elegant series of experiments using retroviral lineage-tracing has provided strong evidence that ventricular components of the conduction system are derived from cardiomyogenic cells (Gourdie et al., 1995; Cheng et al., 1999). In addition, it has been suggested that the differentiation of a subset of Purkinje fibers, adjacent to the arterial bed, might be regulated by local signals from the coronary artery (Gourdie et al., 1995). It was subsequently shown that endo-

thelin-1, a paracrine factor secreted by endothelial cells, is capable of inducing embryonic chick myocytes to the cells of the CCS.

In contrast to the avian CCS, the ventricular CCS in most mammals is morphologically and topologically different from that of chick as it is mainly subendocardial. Hence, the developmental role of the coronary artery in mammalian CCS differentiation is uncertain. In the murine heart, the expression of several markers, including specific connexins and *lacZ* under the transcriptional regulation of either the *minK* or *HF-1b* loci, delineate the bundle branches and proximal Purkinje fibers, but none appear to delineate the full extent of the conductive network along the ventricular free walls (Delorme et al., 1995; Coppen et al., 1998, 1999; Kupershmidt et al., 1999; Nguyen-Tran et al., 2000). In contrast, the entire mouse CCS, including the distal Purkinje fiber network, in both embryonic and neonatal hearts has been visualized recently by way of β-galactosidase (β-gal) reporter activity (Rentschler et al., 2001) in the *CCS-lacZ* mouse line. Recently, the β-gal–positive cells in the interventricular septum (IVS) region of the *CCS-lacZ* adult mice have been reported to correspond to the Cx40-positive cells (Myers and Fishman, 2004). However, the comparison was performed by using serial sections; thus, further clarification is needed to determine whether the same cell expresses the both markers or not. Nevertheless, it is considered that the β-gal–positive cells of *CCS-lacZ* embryos are the most reliable indication for CCS cells in the mouse embryo, compared with the other markers. Although the lineage of the cells of the murine CCS is incompletely characterized, a recent study demonstrated that exogenous treatment of 8.5–10.5 days postcoitum (dpc) embryos with neuregulin-1, an endocardial-derived growth and differentiation factor essential for ventricular trabeculation, could induce a CCS-like phenotype in embryonic cardiomyocytes (Rentschler et al., 2002). Whereas, the use of in vitro culture systems has demonstrated also that the treatment of embryonic stem cells with endothelin-1 but not with neuregulin-1 increased the percentage of pacemaker-like

cells, suggesting that the role of endothelin-1 in CCS development may be conserved, even in mice (Gassanov et al., 2004).

Mesp1 and Mesp2 are transcription factors that contain almost identical basic helix–loop–helix (bHLH) motifs and are encoded by genes that both localize in chromosome 7 (Saga et al., 1996, 1997). Disruption of the *Mesp1* gene results in cardia bifida (Saga, 1998). We also have shown previously, using double knockout mouse embryos and by chimera analysis, that *Mesp1* and *Mesp2* are essential for the development of cardiac mesoderm (Kitajima et al., 2000). *Mesp1* expression is restricted to the nascent mesodermal cells, and its expression is transient and down-regulated before heart tube formation (Saga et al., 1999). However, lineage analysis using *Mesp1-cre* has revealed that *Mesp1*-expressing cells are incorporated into almost all of the precursors of the cardiovascular system (i.e., endothelium, endocardium, myocardium, and epicardium), both in embryonic and extraembryonic regions at 9.5 dpc, and that *Mesp1* expression is the earliest detectable molecular marker in heart precursor cells (Saga et al., 1999, 2000). In this current study, we describe further detailed lineage analyses of the mouse heart using *Mesp1-cre* mice. We show that *Mesp1*-nonexpressing cells contribute to neural crest-derived regions as well as to a subset of the cells in the ventricular CCS.

RESULTS

Lineage Analysis of *Mesp1*-Expressing Mesodermal Cells in the Developing Heart

Using *Mesp1-cre*–mediated cell lineage analysis, we previously reported that *Mesp1*-expressing cells were incorporated into almost all precursors of the cardiovascular system in both embryonic and extraembryonic regions at 9.5 dpc (Saga et al., 2000). However, further analysis at 13.5 dpc now has revealed that the cardiogenic cells are not entirely contributed by *Mesp1*-expressing cells, suggesting that the origin of these cells may be subdivided according to *Mesp1* expression (Fig. 1A–C). At this developmen-
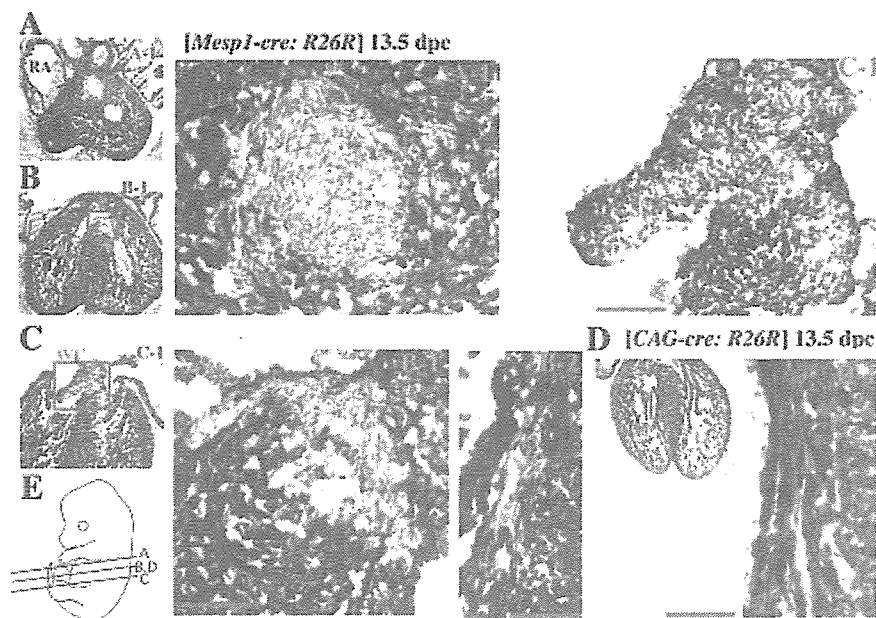
Fig. 1. Transverse sections of β-galactosidase (β-gal) -stained *Mesp1-cre:R26R* or *CAG-cre: R26R* embryos at 13.5 days post coitum (dpc). A–B: The β-gal–negative areas were observed in the region of outflow tract cushions (OTC; A; boxed area in A-1) and along the interventricular septum (IVS) in a pattern reminiscent of the ventricular cardiac conduction system (CCS; B; boxed areas, B-1 and B-2). C: atrioventricular cushions (AVC; boxed area in C-1) showed β-gal activity. Original magnification, ×100. Magnified images of OT cushion cells, the interventricular regions, and AV cushions are shown in A-1, B-1 and -2, and C-1, respectively. D: Transverse sections of β-gal–stained *CAG-cre:R26R* embryos show no β-gal–negative regions, suggesting that *R26R* expression was not shut down as *Mesp1*-nonexpressing cells differentiate. A magnified image in the interventricular regions is shown in D-1. E: Sectioning planes are illustrated and were counterstained with eosin. LV, left ventricle; RA, right atrium; RV, right ventricle. Scale bar = 100 μm.
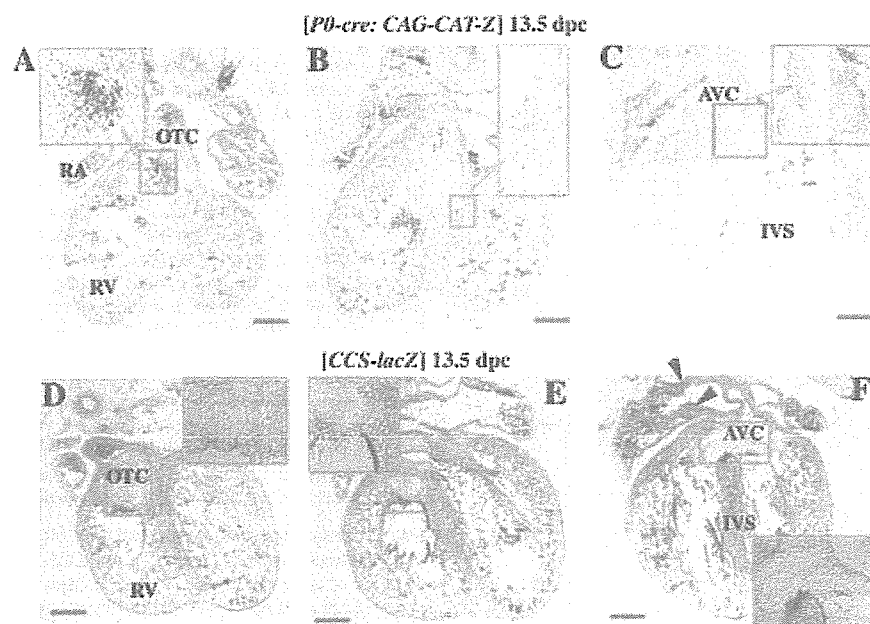

Fig. 2. β-galactosidase (β-gal) staining in sections of the *P0-cre:CAG-CAT-Z* and the *CCS-lacZ* embryos at 13.5 days post coitum (dpc). A–C: In the *P0-cre:CAG-CAT-Z* embryo, high β-gal activity is observed in the region of the outflow tract cushion (OTC; A, boxed area), but little activity is evident in the region of the atrioventricular cushion (AVC; C, boxed area). Original magnification, ×40. Note that the β-gal activity was not observed within the ventricle and the interventricular septum (IVS; B). D–F: The images in the boxed area are magnified. In the *CCS-lacZ* embryo, β-gal activity is observed strongly in part of the atria (indicated by arrowheads) and along the IVS in a pattern reminiscent of the ventricular cardiac conduction system (CCS; boxed area). In contrast, β-gal activity in either the OTC or AVC regions was barely detectable (D,F). The images in the boxed area are magnified. Sectioning planes of images A–C and D–F are the same as those illustrated in Figure 1E: A–C, respectively. All sections were counterstained with eosin. RA, right atrium; RV, right ventricle. Scale bar = 200 μm.

tal stage (13.5 dpc), during which the septation complexes start to form, *Mesp1*-nonexpressing cells are also visible along the IVS region in a pattern reminiscent of the AVB and bundle branches, which are components of the ventricular CCS (Fig. 1B). In addition, region of the OT cushions had little β-gal activity (Fig. 1A), unlike most of the AV cushions that had strong activity (Fig. 1C). In the *CAG-cre* mouse, in which the *cre* gene is under the control of the cytomegalovirus immediate early enhancer-chicken beta-actin hybrid (*CAG*) enhancer, it has been reported that the sequence between the two *loxP* sites is deleted in all tissues in the mouse embryo (Sakai and Miyazaki, 1997). This finding was confirmed in our current experiments; all of the cells in the developing heart of double-transgenic embryos were positive for *LacZ* (Fig. 1D), indicating that this expression is not down-regulated upon *CAG* promoter activation. This observation strongly suggests that *Mesp1*-"non" expressing cells are indeed present in the developing murine heart of the *Mesp1-cre:R26R* reporter double-transgenic mouse.

Because neural crest cells are known to contribute to part of the developing heart structure (Jiang et al., 2000), we initially expected that the regions containing *Mesp1*-nonexpressing cells might reflect this population. To address this possibility more fully, we next compared our findings with a previous report that used a *P0-cre* transgene and *CAG-CAT-Z* reporter gene to identify neural crest-derived cells (Yamauchi et al, 1999).

Mesp1-Nonexpressing Cells Along the Ventricular Septum Are Not Derived From the Neural Crest

We analyzed *P0-cre:CAG-CAT-Z* embryos to examine whether neural crest cells indeed contribute to any of the regions occupied by *Mesp1*-nonexpressing cells. In the *P0-cre:CAG-CAT-Z* embryo at 13.5 dpc, β-gal activity was mainly detected in the mesenchyme located within the OT cushions of the heart (Fig. 2A), which is consistent with previous findings (Yamauchi et al., 1999) and a report using *Wnt1-cre* mice (Jiang et al.,
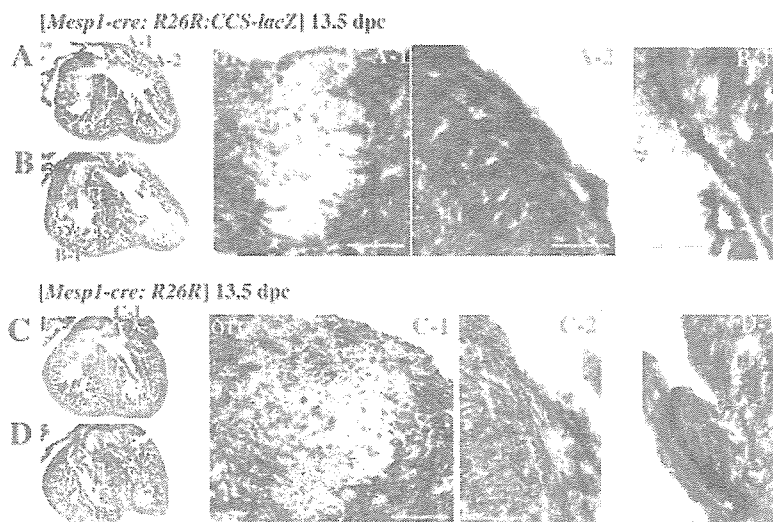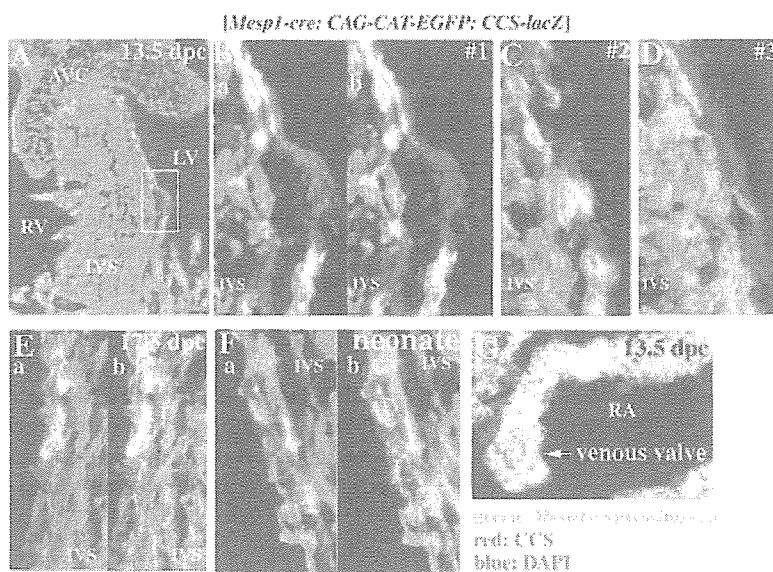
[Mesp1-cre: R26R:CCS-lacZ] 13.5 dpc

Fig. 3.

[Mesp1-cre: CAG-CAT-EGFP: CCS-lacZ]

Fig. 4.
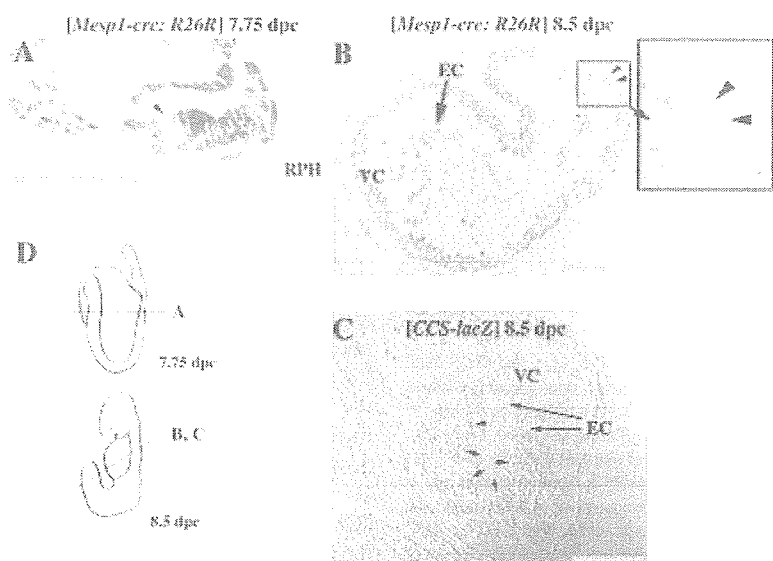
[Mesp1-cre: R26R] 7.75 dpc   [Mesp1-cre: R26R] 8.5 dpc

Fig. 5.

Fig. 3. Comparison of β-gal staining patterns between Mesp1-cre:R26R:CCS-lacZ triple hetero-embryos and Mesp1-cre:R26R embryos. A,B: Sections of the heart of the Mesp1-cre: R26R:CCS-lacZ embryo at 13.5 days post coitum (dpc). C,D: Compared with the Mesp1-cre: R26R embryo (boxes in C-2 and D-1), Mesp1-nonexpressing cells along the interventricular (IVS) were barely observed in the Mesp1-cre: R26R:CCS-lacZ triple hetero-embryos (A,B; boxes in A-2 and B-1). However, Mesp1-nonexpressing cells in outflow tract (OT) cushion regions were also detected, even in the triple hetero-embryos (box A-1). Original magnification, ×100. The images in the boxed area are magnified. Sectioning planes of A, B, and C, D are the same as those illustrated in Figure 1E: B and C, respectively. Sections were counterstained with eosin. AVC, atrioventricular cushion; IVS, interventricular septum; RA, right atrium; RV, right ventricle; Scale bar = 100 μm.

Fig. 4. Mesp1-nonexpressing cells contribute to a subset of the ventricular cardiac conduction system (CCS). Triple immunostaining for Mesp1-expressing cells (green fluorescent protein [GFP] -positive cells; green), cells of the ventricular CCS (LacZ-positive cells; red), and nuclei (4′,6′-diamidino-2-phenylindole [DAPI] staining; blue) in a Mesp1-cre:CAG-CAT-EGFP:CCS-lacZ embryo. All images shown are merged views, and double immunostaining of GFP and LacZ (a) and a triple immunostaining image with additional DAPI staining (b) are shown in some cases. A–D: A merged view of the interventricular (IVS) region at 13.5 days post coitum (dpc). The boxed area of the ventricular CCS in A was magnified as shown in B. Other sections derived from additional embryos are shown in C and D. The presence of red cells suggests that Mesp1-nonexpressing cells actually belong to the ventricular CCS, whereas some Mesp1-expressing cells also colocalize here (yellow). Typical images of mixed cell populations are shown in B and C, whereas a red cell-dominant section is shown in D. Original magnification, ×400, except for A, which is ×100. E,F: Merged view in the IVS region in an embryo at 17.5 dpc (E) or in a neonate (F). Original magnification, ×400. Red cells (i.e., the Mesp1-nonexpressing cells belonging to the CCS) were observed even at later stages beyond 13.5 dpc. G: The region of the venous valves, which are proposed remnants of the embryonic sinoatrial (SA) ring, at 13.5 dpc. Almost all of the cells in this region were stained yellow, suggesting that the cells belonging to the venous valves are Mesp1-expressing. Original magnification, ×200. Sectioning planes are those between B and C, illustrated in Figure 1E. AVC, atrioventricular cushion; LV, left ventricle; OTC, outflow tract cushion; RA, right atrium; RV, right ventricle.

Fig. 5. Comparison of transverse sections of β-gal stained Mesp1-cre:R26R embryos with CCS-lacZ embryos at an earlier stage. A: At 7.75 days post coitum (dpc) in Mesp1-cre:R26R embryos, we observed a few Mesp1-nonexpressing cells within the primitive heart tube (arrow head). Original magnification, ×400. B: At 8.5 dpc, the regions of the Mesp1-nonexpressing cells in Mesp1-cre:R26R embryos, were observed more clearly (arrowheads). C: The β-gal–positive regions (i.e., the cells belonging to the CCS) were observed mainly in the subendocardial myocardium of 8.5 dpc CCS-lacZ mouse (arrows). Original magnification, ×200. D: Sectioning planes are illustrated. Sections were counterstained with eosin. EC, endocardium; RPH, right primitive heart tube; VC, ventricular chamber. Scale bars = 100 μm.

2000). There were only minimal contributions by neural crest cells in the AV cushions, as predicted by the β-gal activity in the *Mesp1-cre:R26R* mouse (Fig. 2C). Importantly, however, neural crest-derived mesenchyme was not observed in either part of the ventricle or the IVS (Fig. 2B), where *Mesp1*-nonexpressing cells were visible (Fig. 1B). This finding indicates that other cell types must contribute to this particular region. Intriguingly, the distribution of *Mesp1*-nonexpressing cells resembled that of the AVB and bundle branches and also the Purkinje fibers of the CCS. This prompted us to speculate that ventricular CCS cells might be derived from lineages that are distinct from both the neural crest and *Mesp1*-expressing mesodermal cells.

Mesp1-Nonexpressing Cells Contribute to the CCS

As a preliminary approach to determine whether or not *Mesp1*-nonexpressing cells did in fact reside in the CCS, we compared these cells with the β-gal expression patterns in embryonic hearts of *CCS-lacZ* transgenic mice. In these mice, the specialized CCS can be visualized by β-gal activity (Rentschler et al., 2001). In 13.5 dpc hearts from these transgenic animals, strong β-gal activity could be observed in part of the atrium, which could correspond to the SA node. This high level of activity could also be detected along the IVS, which demarcates the ventricular CCS, including the AVB and bundle branches (Fig. 2D–F). When comparing these results with those shown in Figure 1, the portion of the *Mesp1*-nonexpressing cell population along the IVS was found to show a similar pattern to the β-gal-positive regions in the *CCS-lacZ* mice, suggesting that these *Mesp1*-nonexpressing cells contribute to the ventricular CCS.

To provide direct evidence for our hypothesis that cells of the ventricular CCS are indeed derived from *Mesp1*-nonexpressing cells, we generated triple transgenic *Mesp1-cre:R26R:CCS-lacZ* mice. Because both the *CCS-lacZ* and *R26R* transgenic mice use β-gal as a marker, the entire region contributed by the *Mesp1*-nonexpressing cells in the IVS would become β-gal–positive in the triple hetero-embryonic

hearts if our contention was correct. As shown in Figure 3, this was found to be the case, as all of the cells in the IVS had β-gal activity, which was in contrast to the corresponding sections of the *Mesp1-cre:R26R* embryo (Fig. 3C,D). Moreover, the region of the OT cushions had little β-gal activity even in the triple hetero-embryo (Fig. 3A), supporting our conclusion that this region is occupied mainly by cells of neural crest origin. Hence, these data suggest that the *Mesp1*-nonexpressing cells in the IVS belong to the ventricular CCS.

It was still unclear, however, whether all of the ventricular CCS is derived from *Mesp1*-nonexpressing cells, because both the *CCS-lacZ* and *R26R* reporter mice use the same β-gal marker. We, therefore, performed a similar series of studies using the *CAG-CAT-EGFP* strain (Kawamoto et al., 2000), in which GFP expression is dependent upon cre-mediated recombination and representative results are shown in Figure 4. *Mesp1*-nonexpressing cells at 13.5 dpc do indeed reside within the ventricular CCS (*Mesp1*-nonexpressing/*CCS-lacZ*-positive red cells in Fig. 4A–D), although it is clear that the CCS is also observed in the *Mesp1*-expressing cell populations (i.e., *Mesp1*-expressing/*CCS-lacZ*–positive yellow cells). In addition, after 4',6'-diamidino-2-phenylindole (DAPI) staining, we observed that all of the green fluorescent protein (GFP) -negative *Mesp1*-nonexpressing cells belonged to the lacZ-positive cells of the ventricular CCS, because cells positive for DAPI alone (blue) were rarely observed along the IVS (b in Fig. 4A–C). To demonstrate the heterocellular origin of CCS more unequivocally and to analyze the ratios quantitatively, we generated serial sections of the embryonic heart along the anteroposterior axis and analyzed the staining patterns.

A total of three embryos were sectioned and 58 sections containing CCS-LacZ staining in the IVS region were further subjected to semiquantitative analysis (Supplementary Figure S1, which can be viewed at http://www.interscience.wiley.com/jpages/1058-8388/suppmat). However, as the CCS distributes peripherally in the IVS with multiple branchings, it is very difficult to quantify. We, there-

fore, roughly estimated the ratio by counting DAPI stained nuclei in each cell type and selected 28 typical sections, from which 16 showed a colocalization pattern for yellow and red cells (Fig. 4B,C). Of these 16 sections, 2 and 5 showed a red cell- and a yellow cell-dominant pattern, respectively (Fig. 4D, and data not shown). We have estimated that approximately 20% of the ventricular CCS, along the IVS, corresponds to *Mesp1*-nonexpressing cells. Moreover, red cells (i.e., the *Mesp1*-nonexpressing cells belonging to the ventricular CCS) were also observed in the ventricular CCS even at later developmental stages of 17.5 dpc (Fig. 4E) and in neonates at 4 days after birth (Fig. 4F). The AV cushion cells were weakly positive for the GFP signal, due to the thinness of the cytoplasm and resulting lower intensity of fluorescence (Fig. 4A), but their identity was confirmed by LacZ staining in *Mesp1-cre; R26R* embryos (Fig. 1C). Thus, we conclude unequivocally that the population of *Mesp1*-nonexpressing cells, which we identified along the ventricular septum, contributes to the CCS.

In the case of the SA or AV node regions of the CCS, the contribution of *Mesp1*-expressing and/or *Mesp1*-nonexpressing cells was not as clear from our present results using embryos at 13.5 dpc, because these typical node structures were not discernible. In contrast, we were able to determine that most of the cells in the venous valves, which are the proposed remnants of the embryonic SA ring in the fully developed heart (Rentschler et al., 2001), of the *Mesp1-cre:CAG-CAT-EGFP:CCS-lacZ* embryo were *Mesp1*-expressing (i.e., GFP–positive cells). This determination was revealed by the *Mesp1*-expressing/*CCS-lacZ*–positive yellow cells at 13.5 dpc (Fig. 4G). However, the developmental relationships between the venous valves and both the SA and AV nodes have not yet been determined.

Origin of *Mesp1*-Nonexpressing Cells

To determine the origin of the *Mesp1*-nonexpressing cells, we examined the LacZ expression profiles in more immature *Mesp1-cre:R26R* and *CCS-lacZ* embryos. As shown in Figure 5A,

even at 7.75 dpc, at which stage the cardiac crescent can be observed, a few β-gal–negative cells were detectable in the *Mesp1-cre:R26R* embryo. The β-gal–negative cells were observed in the myocardium region more clearly at 8.5 dpc (Fig. 5B). In the *CCS-lacZ* embryo, although the heart region at 7.75 dpc was confirmed to be β-gal–negative (data not shown) as reported previously (Rentschler et al., 2001), patchy staining was observed mainly in the subendocardial myocardium region at 8.5 dpc (Fig. 5C). However, a direct relationship between the *Mesp1*-nonexpressing cells and the CCS cells is still not clear, although the neural crest cells, which are also identifiable as *Mesp1*-nonexpressing cells in our system, have not yet arrived in the heart at this stage and can be excluded (Jiang et al., 2000).

DISCUSSION

In this study, we have found using a Cre-loxP site-specific recombination system that the origin of the cardiac mesenchyme is subdivided according to the presence of *Mesp1* expression. We demonstrate that the regions occupied by *Mesp1*-nonexpressing cells correspond to two distinct populations of cells: one derived from the neural crest and the other one that contributes to the ventricular CCS.

Comparison of the Cell-Lineages of Neural Crest Cells and *Mesp1*-Nonexpressing cells

In our experiments with *Mesp1-cre:R26R* embryos, we have found that cells derived from the neural crest are negative but that mesodermal cells derived from *Mesp1*-expressing cells are positive, for β-gal activity. We have also confirmed that mammalian cardiac neural-crest cells are *Mesp1*-negative (Figs. 1, 2) and contribute to the mesenchyme in the OT cushions of the heart. These observations were made following neural crest cell lineage analyses using the *P0-cre:CAG-CAT-Z* strain (Fig. 2) and are consistent with previous results obtained using *Wnt1-cre:R26R* double transgenic mice (Jiang et al., 2000). The origin of the cells of the AV cushions was suggested to be mesodermal, because this region was occupied by *Mesp1*-expressing cells in our study

(Fig. 1C). This result is consistent with the previous study of Kisanuki et al. (2001) using *Tie2-cre* mice that reported that the origin of the AV cushions is mainly of endocardial cell lineage. Thus, mesenchymal cells in the OT cushions are derived from mainly neural crest cells and those in the AV cushions are derived from endocardium.

Importantly, we observed a second population of *Mesp1*-nonexpressing cells, along the IVS (Fig. 1B). Because this region is not contributed by neural crest cells (Fig. 2B), we explored the possibility that these *Mesp1*-nonexpressing cells reside in the ventricular CCS. Before examining this possibility, we first confirmed that the failure to express β-gal in the *Mesp1-cre:R26R* embryos was not due to an artifact, such as down-regulation of *LacZ* expression during differentiation or mosaicism of Cre recombinase expression. To exclude the former possibility, we examined *CAG-cre:R26R* mice, in which Cre recombinase is ubiquitously expressed and all cells should be *LacZ*-positive. We did not subsequently observe any *LacZ*-negative cells in the heart, indicating that there had been no down-regulation of *LacZ* upon cell differentiation (Fig. 1D). To exclude possible mosaicism of Cre recombinase, we repeated our analysis in more than 20 embryos and observed very consistent results, although some clonal differences may exist. In addition, when we crossed the *Mesp1-cre* and *CCS-lacZ* strains and monitored *R26R*-dependent reporter gene expression, we did not observe patchy *LacZ*-negative cells in the ventricular wall. Thus, it appears unlikely that mosaicism of the *R26R* reporter could account for our results.

As for the contribution of the neural crest cells into the ventricular CCS, it was reported that neural crest-derived cells were observed in the vicinity of the CCS in the IVS at 14.5 dpc using the *Wnt1-cre:R26R* reporter system (Poelmann et al., 2004). Thus, the possibility cannot be rule out that the neural crest cells contribute to CCS in the IVS, although we could not detect any β-gal–positive cells in the IVS in our *P0-cre:CAG-CAT-Z* system. The discrepancy could be due to the difference in systems used for lineage analyses. The future studies using triple transgenic strategy (*Wnt1-cre:CAG-*

CAT-GFP:CCS-lacZ) as used in our current study would be useful to discriminate the discrepancy.

Origins of the CCS

Using *Mesp1-cre:R26R* embryos, we identified a population of *Mesp1*-nonexpressing cells that were found to be distributed in the wall along the ventricular septum (Fig. 1B). The results of genetic crosses with the *CCS-lacZ* strain suggested that these *Mesp1*-nonexpressing cells contribute to the ventricular CCS (Fig. 3B). To confirm these findings, we generated triple transgenic *Mesp1-cre:CAG-CAT-EGFP:CCS-lacZ* mice. Double-staining for GFP and β-gal expression and/or additional DAPI staining in these mice confirmed that the *Mesp1*-nonexpressing cells contribute approximately 20% of the ventricular CCS (Fig. 4). Moreover, these populations of cells can be distinguished at a stage as early as stage 7.75 dpc at least (Fig. 5), whereas *Mesp1* is initially, albeit transiently, expressed at 6.5 dpc (Saga et al., 1996).

The pacemaking and conduction systems of the heart are composed of the SA node, AV node, AVB, the bundle branches, and the Purkinje fibers, each of which can be distinguished morphologically, functionally, and molecularly (Moorman and Christoffels, 2003). The origin of the nodal tissue is less clear than that of the ventricular CCS, although the primary myocardium is suggested to be a candidate (Moorman and Christoffels, 2003). Recently, it was suggested that some of the working myocardium could also differentiate into nodal tissues, even after birth (Pashmforoush et al., 2004). Although the developmental relationships between the venous valves and the nodes have not yet been fully elucidated, our data indicate that most of cells in the venous valves, which are proposed to be remnants of the embryonic SA ring (Rentschler et al., 2001), are derived from *Mesp1*-expressing cells (Fig. 4G). However, further detailed studies will be required to determine the precise cellular origin of the nodes and their relationships with the venous valves.

In the present analyses, we have focused on the cell-lineages of the ventricular CCS and shown them to be of
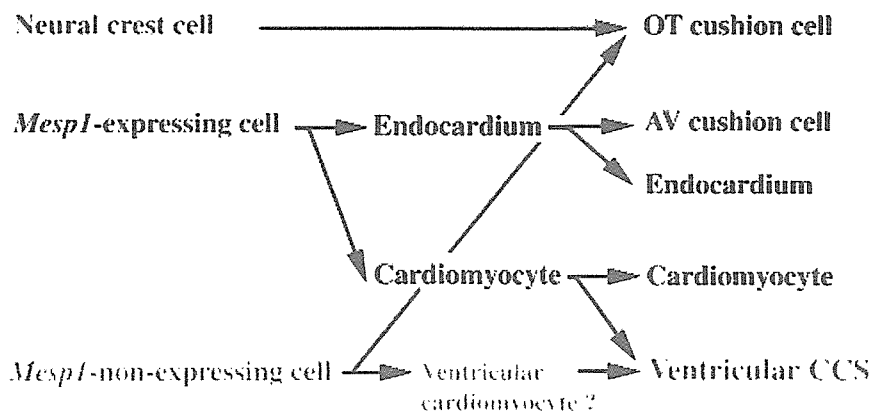
Fig. 6. Summary of the origin and cell-fate relationships of cardiac mesenchyme cell types. Each cardiac cell type is established by three distinct origins: neural crest cells, the mesodermal cells of *Mesp1*-expressing cells, and *Mesp1*-nonexpressing cells. It is noteworthy that both the *Mesp1*-expressing cells and the *Mesp1*-nonexpressing cells contribute to the ventricular CCS. In addition, the origins of the subset of the ventricular CCS that are contributed by the *Mesp1*-nonexpressing cells are distinguishable from that of the myocardium by the *Mesp1* expression profile. We speculate that the *Mesp1*-nonexpressing cardiomyocyte may be a candidate for the origin of the subset of the ventricular CCS. [Color figure can be viewed in the online issue, which is available at www.interscience.wiley.com.]

heterocellular origin. Two possibilities have emerged from both our analyses and previous reports concerning the origin of the ventricular CCS in mouse, occupied by *Mesp1*-nonexpressing cells. First, it is conceivable that the *Mesp1*-nonexpressing cells in the CCS are not derived from cardiomyocytes. Alternatively, these cells may represent cardiomyocytes, which simply do not express *Mesp1*. We favor this latter possibility. Lineage tracing experiments in chick have convincingly demonstrated that the ventricular CCS, including the Purkinje fibers, are derived from cardiomyocytes (reviewed in Mikawa, 1999; Pennisi et al., 2002). Moreover, experiments in the mouse also indicate that embryonic cardiomyocytes can be converted to a CCS-like phenotype in response to neuregulin-1, at least when assayed by up-regulation of the CCS-lacZ transgene (Rentschler et al., 2002). Nonetheless, additional analyses will be required to determine the basis for the molecular heterogeneity within the ventricular CCS and to determine whether there is associated functional diversity in this structure.

In conclusion, we have determined that *Mesp1*-nonexpressing cells contribute to the ventricular CCS in addition to the OT cushion. Furthermore, we indicate a possibility that a population of the cells that contribute to the ventricular CCS might be distinguished at an early stage of de-

velopment. Unfortunately, it could not be clarified from our present experiments whether *Mesp1*-nonexpressing cells also contributed to the other regions of the CCS, such as the SA or AV nodes. A scheme summarizing the cell lineage relationships in the developing murine heart is shown in Figure 6. Our observation that the ventricular CCS includes both *Mesp1*-expressing and -nonexpressing cells is evidence of the heterogeneous nature of the ventricular CCS. The further identification of specific molecular markers for the mouse CCS, expressed at early embryonic stages, will undoubtedly enhance our understanding of the developmental biology of the CCS in the heart.

EXPERIMENTAL PROCEDURES

Lineage Analysis of *Mesp1*-Expressing Cells

The *Mesp1-cre* knockin mouse was constructed by introduction of a gene encoding Cre recombinase into the *Mesp1* locus, as previously described (Saga et al., 1999). The fidelity of expression was confirmed by in situ hybridization at E7.0 (data not shown). Genotyping was performed by polymerase chain reaction using a neo-specific primer NeoAL2: 5'-GGGGATGCGGTGGGCT-CTATGGCTT-3' and *Mesp1* primer MesP1-GR1: 5'-ATATGCCAAGTCATT-GAGGTGAGCTTTC-3'. *Mesp1-cre* mice

were crossed with either *CAG-CAT-Z* (Araki et al., 1995), *R26R* (Soriano, 1999), or *CAG-CAT-EGFP* (Kawamoto et al., 2000) reporter mice. *P0-cre* (Yamauchi et al., 1999) and *CCS-lacZ* mice (Rentschler et al., 2001) were also used for cell lineage analyses. Mice were maintained on a 7:00 AM to 7:00 PM light–dark cycle, with noon on the day of vaginal plug discovery defined as 0.5 dpc.

β-gal Staining, Immunostaining, and In Situ Hybridization

Embryos that had been fixed at 7.5–10.5 dpc were stained for the detection of β-galactosidase activity in whole-mounts as described previously (Saga et al., 1992). The specimens were then dehydrated by means of a graded ethanol series, embedded in either paraffin wax or plastic resin (technovit 8100, Heraeus Kulzer, Inc.) and sectioned at a thickness of 4 μm. Hearts that had been isolated from embryos at later stages were subjected to β-gal staining after sectioning. Briefly, hearts were fixed in a solution of 2% paraformaldehyde, 0.05% glutaraldehyde, and 0.02% NP-40 in phosphate buffer (PBS) for 30 min on ice. The tissues were then sequentially soaked in a graded series of 10, 20, and 30% sucrose (w/v) in PBS while being gently agitated on a shaking platform, culminating in a 50:50 mix of 30% sucrose:OCT. Samples were frozen and stored at −80°C until sectioning at 8 μm thickness, and the sections were placed on gelatin-coated slides. Frozen sections of *Mesp1-cre:CAG-CAT-EGFP:CCS-lacZ* mouse hearts was stained with anti-lacZ and anti-GFP antibodies as follows: sections prepared were fixed with 4% paraformaldehyde for 3 min, treated with 10 μg/ml proteinase K and blocked in 3% skim milk for 30 min at room temperature (RT). Blocking solutions was replaced with rabbit anti-β-gal antibody (Cappel, ICN Pharmaceuticals, Inc., OH) at a dilution of 1:2,000 and with rat anti-GFP antibody (Nacalai Tesque, Kyoto, Japan) at a dilution 1:200 and incubated overnight at 4°C. After brief washes in PBS, the sections were incubated with Alexa 594–conjugated anti-rabbit followed by Alexa 488–conjugated anti-rat secondary antibodies at dilutions of 1:200

for 90 min at RT. These sections were then incubated with 0.1 μg/ml of DAPI (Sigma, St. Louis, MO) for 5 min to visualize nuclei.

REFERENCES

Araki K, Araki M, Miyazaki J, Vassalli P. 1995. Site specific recombination of a transgene in fertilized eggs by transient expression of Cre recombinase. Proc Natl Acad Sci U S A 92:160–164.

Cheng G, Litchenberg WH, Cole GJ, Mikawa T, Thompson RP, Gourdie RG. 1999. Development of the cardiac conduction system involves recruitment within a multipotent cardiomyogenic lineage. Development 126:5041–5049.

Coppen SR, Dupont E, Rothery S, Severs NJ. 1998. Connexin45 expression is preferentially associated with the ventricular conduction system in mouse and rat heart. Circ Res 82:232–243.

Coppen SR, Severs NJ, Gourdie RG. 1999. Connexin45 (alpha 6) expression delineates an extended conduction system in the embryonic and mature rodent heart. Dev Genet 24:82–90.

Delorme B, Dahl E, Jarry-Guichard T, Marics I, Briand JP, Willecke K, Gros D, Theveniau-Ruissy M. 1995. Developmental regulation of connexin 40 gene expression in mouse heart correlates with the differentiation of the conduction system. Dev Dyn 204:358–371.

Gassanov N, Er F, Zagidullin N, Hoppe UC. 2004. Endothelin induces differentiation of ANP-EGFP expressing embryonic stem cells towards a pacemaker phenotype. FASEB J 18:1710–1712.

Gourdie RG, Mima T, Thompson RP, Mikawa T. 1995. Terminal diversification of the myocyte lineage generates Purkinje fibers of the cardiac conduction system. Development 121:1423–1431.

Jiang X, Rowitch DH, Soriano P, McMahon AP, Sucov HM. 2000. Fate of the mammalian cardiac neural crest. Development 127:1607–1616.

Kawamoto S, Niwa H, Tashiro F, Sano S, Kondoh G, Takeda J, Tabayashi K, Miyazaki J. 2000. A novel reporter mouse strain that expresses enhanced green fluorescent protein upon Cre-mediated recombination. FEBS Lett 470: 263–268.

Kirby ML, Gale TF, Stewart DE. 1983. Neural crest cells contribute to normal aorticopulmonary septation. Science 220: 1059–1061.

Kisanuki YY, Hammer RE, Miyazaki J, Williams SC, Richardson JA, Yanagisawa M. 2001. Tie2-Cre transgenic mice: a new model for endothelial cell-lineage analysis in vivo. Dev Biol 230:230–242.

Kitajima S, Takagi A, Inoue T, Saga Y. 2000. MesP1 and MesP2 are essential for the development of cardiac mesoderm. Development 127:3215–3226.

Kupershmidt S, Yang T, Anderson ME, Wessels A, Niswender KD, Magnuson MA, Roden DM. 1999. Replacement by homologous recombination of the minK gene with lacZ reveals restriction of minK expression to the mouse cardiac conduction system. Circ Res 84:146–152.

Mikawa T. 1999. Cardiac lineages. In: Harvey RP, Rosenthal N, editors. Heart development. San Diego: Academic Press. p 19–33.

Moorman AFM, Christoffels VM. 2003. Cardiac chamber formation: development, genes, and evolution. Physiol Rev 83:1223–1267.

Moorman AFM, deJong F, Denyn MM, Lamers WH. 1998. Development of the cardiac conduction system. Circ Res 82: 629–644.

Myers DC, Fishman GI. 2004. Toward an understanding of the genetics of murine cardiac pacemaking and conduction system development. Anat Rec A Discov Mol Cell Evol Biol 280:1018–1021.

Nguyen-Tran VT, Kubalak SW, Minamisawa S, Fiset C, Wollert KC, Brown AB, Ruiz-Lozano P, Barrere-Lemaire S, Kondo R, Norman LW, et al. 2000. A novel genetic pathway for sudden cardiac death via defects in the transition between ventricular and conduction system cell lineages. Cell 102:671–682.

Pashmforoush M, Lu JT, Chen H, Amand TS, Kondo R, Pradervand S, Evans SM, Clark B, Feramisco JR, Giles W, Ho SY, Benson DW, Silberbach M, Shou W, Chien KR. 2004. Nkx2-5 pathways and congenital heart disease; loss of ventricular myocyte lineage specification leads to progressive cardiomyopathy and complete heart block. Cell 117:373–386.

Pennisi DJ, Rentschler S, Gourdie RG, Fishman GI, Mikawa T. 2002. Induction and patterning of the cardiac conduction system. Int J Dev Biol 46:765–775.

Poelmann RE, Jongbloed MR, Molin DG, Fekkes ML, Wang Z, Fishman GI, Doetschman T, Azhar M, Gittenberger-de Groot AC. 2004. The neural crest is contiguous with the cardiac conduction system in the mouse embryo: a role in induction? Anat Embryol (Berl) 208:389–393.

Rentschler S, Vaidya DM, Tamaddon H, Degenhardt K, Sassoon D, Morley GE, Jalife J, Fishman GI. 2001. Visualization and functional characterization of the developing murine cardiac conduction system. Development 128:1785–1792.

Rentschler S, Zander J, Meyers K, France D, Levine R, Porter G, Rivkees SA, Morley GE, Fishman GI. 2002. Neuregulin-1 promotes formation of the murine cardiac conduction system. Proc Natl Acad Sci U S A 99:10464–10469.

Saga Y. 1998. Genetic rescue of segmentation defect in MesP2-deficient mice by MesP1 gene replacement. Mech Dev 75: 53–66.

Saga Y, Yagi T, Ikawa Y, Sakakura T, Aizawa S. 1992. Mice develop normally without tenascin. Genes Dev 6:1821–1831.

Saga Y, Hata N, Kobayashi S, Magnuson T, Seldin M, Taketo MM. 1996. MesP1: a novel basic helix-loop-helix protein expressed in the nascent mesodermal cells during mouse gastrulation. Development 122:2769–2778.

Saga Y, Hata N, Koseki H, Taketo MM. 1997. Mesp2: a novel mouse gene expressed in the presegmented mesoderm and essential for segmentation initiation. Genes Dev 11:1827–1839.

Saga Y, Miyagawa-Tomita S, Takagi A, Kitajima S, Miyazaki J, Inoue T. 1999. MesP1 is expressed in the heart precursor cells and required for the formation of a single heart tube. Development 126: 3437–3447.

Saga Y, Kitajima S, Miyagawa-Tomita S. 2000. *Mesp1* expression is the earliest sign of cardiovascular development. Trends Cardiovasc Med 10:345–352.

Sakai K, Miyazaki J. 1997. A transgenic mouse line that retains Cre recombinase activity in mature oocytes irrespective of the cre transgene transmission. Biochem Biophys Res Commun 237:318–324.

Soriano P. 1999. Generalized lacZ expression with the ROSA26 Cre reporter strain. Nat Genet 21:70–71.

Waldo K, Miyagawa-Tomita S, Kumiski D, Kirby ML. 1998. Cardiac neural crest cells provide new insight into septation of the cardiac outflow tract: aortic sac to ventricular septal closure. Dev Biol 196: 129–144.

Yamauchi Y, Abe K, Mantani A, Hitoshi Y, Suzuki M, Osuzu F, Kuratani S, Yamamura K. 1999. A novel transgenic technique that allows specific marking of the neural crest cell lineage in mice. Dev Biol 212:191–203.

Premature ovarian failure in androgen receptor-deficient mice

Hiroko Shiina*†‡, Takahiro Matsumoto*‡§, Takashi Sato*, Katsuhide Igarashi¶, Junko Miyamoto*, Sayuri Takemasa*, Matomo Sakari*§, Ichiro Takada*, Takashi Nakamura*§, Daniel Metzger∥, Pierre Chambon∥, Jun Kanno¶, Hiroyuki Yoshikawa†, and Shigeaki Kato*§**

*Institute of Molecular and Cellular Biosciences, University of Tokyo, 1-1-1 Yayoi, Bunkyo-ku, Tokyo 113-0032, Japan; §Exploratory Research for Advanced Technology, Japan Science and Technology, 4-1-8 Honcho, Kawaguchi, Saitama 332-0012, Japan; †Department of Obstetrics and Gynecology, Institute of Clinical Medicine, University of Tsukuba, 1-1-1 Tennoudai, Tsukuba, Ibaraki 305-8575, Japan; ¶Division of Cellular and Molecular Toxicology, National Institute of Health Sciences, 1-18-1 Kamiyoga, Setagaya-ku, Tokyo 158-8501, Japan; and ∥Institut de Genetique et de Biologie Moleculaire et Cellulaire, Centre National de la Recherche Scientifique, Institut National de la Santé et de la Recherche Médicale, Universite Louis Pasteur, College de France, 67404 Illkirch, Strasbourg, France

Premature ovarian failure (POF) syndrome, an early decline of ovarian function in women, is frequently associated with X chromosome abnormalities ranging from various Xq deletions to complete loss of one of the X chromosomes. However, the genetic locus responsible for the POF remains unknown, and no candidate gene has been identified. Using the Cre/LoxP system, we have disrupted the mouse X chromosome androgen receptor (Ar) gene. Female $AR^{-/-}$ mice appeared normal but developed the POF phenotype with aberrant ovarian gene expression. Eight-week-old female $AR^{-/-}$ mice are fertile, but they have lower follicle numbers and impaired mammary development, and they produce only half of the normal number of pups per litter. Forty-week-old $AR^{-/-}$ mice are infertile because of complete loss of follicles. Genome-wide microarray analysis of mRNA from $AR^{-/-}$ ovaries revealed that a number of major regulators of folliculogenesis are under transcriptional control by AR. Our findings suggest that AR function is required for normal female reproduction, particularly folliculogenesis, and that AR is a potential therapeutic target in POF syndrome.

male hormone | nuclear receptor | female physiology | folliculogenesis | kit ligand

Premature ovarian failure (POF) is defined as an early decline of ovarian function after seemingly normal folliculogenesis (1). Genetic causes of POF have been frequently associated with X chromosome abnormalities (1, 2). Complete loss of one of the X chromosomes, as in Turner syndrome, and various Xq deletions are commonly identified as a cause of POF. However, responsible X-linked genes and their downstream targets have not been identified so far.

The androgen receptor (Ar) gene, which is the only sex hormone receptor gene on the X chromosome, is well known to be essential not only for the male reproductive system, but also for male physiology. In contrast, androgens are considered as male hormones; therefore, little is known about androgens' actions in female physiology, although AR expression in growing follicles has been described (3). However, because excessive androgen production in polycystic ovary syndrome causes infertility with abnormal menstrual cycles (4, 5), it is possible that AR-mediated androgen signaling also plays an important physiological role in the female reproductive system. Recently, using Cre/LoxP system, we generated an AR-null mutant mouse line (6) and demonstrated that inactivation of AR resulted in arrest of testicular development and spermatogenesis, impaired brain masculinization, high-turnover osteopenia, and late onset of obesity in males (7–9). At the same time, no overt physical or growth abnormalities were observed in female $AR^{-/-}$ mice. Therefore, to further examine potential role of AR in female physiology, we characterized female reproductive system in $AR^{-/-}$ females. Herein we show that female $AR^{-/-}$ mice develop the POF phenotype. At 3 weeks of age, $AR^{-/-}$ females had

apparently normal ovaries with numbers of follicles similar to those in the wild-type females. However, thereafter the number of healthy follicles in the $AR^{-/-}$ ovary gradually declined, with a marked increase of atretic follicles, and by 40 weeks $AR^{-/-}$ mice became infertile, with no follicle detectable in the ovary. Reflecting this age-dependent progression in ovarian abnormality, several genes known to be involved in the oocyte–granulosa cell regulatory loop were identified by microarray analysis as AR downstream target genes. These findings clearly demonstrate that AR-mediated androgen signaling is indispensable for the maintenance of folliculogenesis and implicate impaired androgen signaling as a potential cause of the POF syndrome.

Materials and Methods

Generation of AR Knockout Mice. AR genomic clones were isolated from a TT2 embryonic stem cell genomic library by using human AR A/B domain cDNA as a probe (6). The targeting vector consisted of a 7.6-kb 5′ region containing exon 1, a 1.3-kb 3′ homologous region, a single loxP site, and a neo cassette with two loxP sites (10). Targeted clones (FB-18 and FC-61) were aggregated with single eight-cell embryos from CD-1 mice (11, 12). Floxed AR mice (C57BL/6) were then crossed with CMV-Cre transgenic mice (6). The two lines exhibited the same phenotypic abnormalities. The chromosomal sex of each pup was determined by genomic PCR amplification of the Y chromosome Sry gene (13).

Western Blot Analysis. To detect AR protein expression, ovarian cell lysates were separated by SDS/PAGE and transferred onto nitrocellulose membranes (14). Membranes were probed with polyclonal AR antibodies (N-20; Santa Cruz Biotechnology), and blots were visualized by using peroxidase-conjugated second antibody and an ECL detection kit (Amersham Pharmacia Biosciences).

Morphologic Classification of Growing Follicles. Sections were taken at intervals of 30 μm, and 6-μm paraffin-embedded sections were mounted on slides. Routine hematoxylin and eosin staining was performed for histologic examination by light microscopy. Follicle numbers in 12 sections per ovary were evaluated as primary follicles (oocyte surrounded by a single layer of cuboidal granulosa cells), preantral follicles (oocyte surrounded by two or
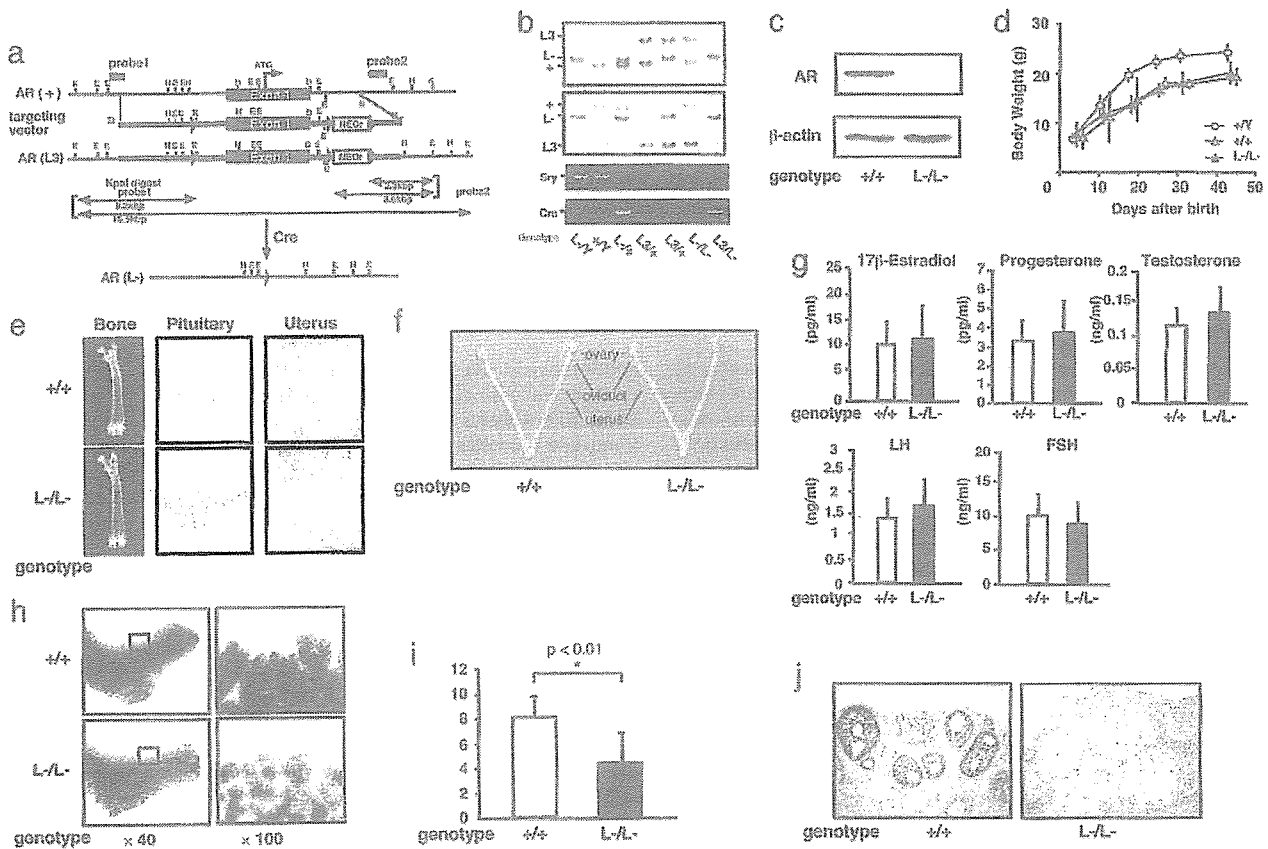
Fig. 1. Phenotypic characterization of AR knockout female mice. (a) Diagram of the wild-type Ar genomic locus (+), floxed AR L3 allele (L3), and AR allele (L-) obtained after Cre-mediated excision of exon 1. K, KpnI; E, EcoRI; H, HindIII; B, BamHI. LoxP sites are indicated by arrowheads. The targeting vector consisted of a 7.6-kb 5′ homologous region containing exon 1, a 1.3-kb 3′ homologous region, a single loxP site, and the neo cassette with two loxP sites. (b) Detection of the Y chromosome-specific Sry gene in $AR^{-/Y}$ mice by PCR. (c) Absence of AR protein in $AR^{-/-}$ mice ovaries by Western blot analysis using a specific C-terminal antibody. (d) Normal weight gain in $AR^{-/-}$ females. (e) Histology of pituitary, uterus, and bone tissues in $AR^{+/+}$ and $AR^{-/-}$ females at 8 weeks of age. (f) Female reproductive organs were macroscopically normal in $AR^{-/-}$ mice. (g) Serum hormone levels at the proestrus stage in $AR^{-/-}$ mice were not significantly altered. Serum 17β-estradiol, progesterone, testosterone, luteinizing hormone (LH), and follicle-stimulating hormone (FSH) levels in $AR^{+/+}$ (n = 13) and $AR^{-/-}$ (n = 10) females at 8–10 weeks of age are shown. (h) Lobuloalveolar development is impaired in $AR^{-/-}$ mammary glands. Whole mount of inguinal mammary glands (Left) and its higher magnification (Right) were prepared on day 3 of lactation. (i) Average number of pups per litter is markedly reduced in $AR^{-/-}$ mice at 8 weeks of age. Data are shown as mean ± SEM and analyzed by using Student's t test. (j) AR immunocytochemistry in $AR^{+/+}$ and $AR^{-/-}$ ovaries. Sections were counterstained with eosin.

more layers of granulosa cells with no antrum), or antral follicles (antrum within the granulosa cell layers enclosing the oocyte). Follicles were determined to be atretic if they displayed two or more of the following criteria within a single cross section: more than two pyknotic nuclei, granulosa cells within the antral cavity, granulosa cells pulling away from the basement membrane, or uneven granulosa cell layers (15).

Immunohistochemistry. Sections were subjected to a microwave antigen retrieval technique by boiling in 10 mM citrate buffer (pH 6.0) in a microwave oven for 30 min (16). The cooled sections were incubated in 1% H_2O_2 for 30 min to quench endogenous peroxidase and then incubated with 1% Triton X-100 in PBS for 10 min. To block nonspecific antibody binding, sections were incubated in normal goat serum for 1 h at 4°C. Sections were then incubated with anti-AR (1:100) or anti-cleaved caspase-3 (1:100) in 3% BSA overnight at 4°C. Negative controls were incubated in 3% BSA without primary antibody. The ABC method was used to visualize signals according to the manufacturer's instructions. Sections were incubated in biotinylated goat anti-rabbit IgG (1:200 dilution) for 2 h at room temperature, washed with PBS, and incubated in avidin–biotin–horseradish peroxidase for 1 h. After thorough washing in PBS, sections were developed with 3,3′-diaminobendizine tetrahydrochloride substrate, slightly counterstained with eosin, dehydrated through an ethanol series and xylene, and mounted.

Estrus Cycles and Fertility Test. To determine the stage of the estrus cycle (proestrus, estrus, and diestrus), vaginal smears were taken every morning and stained with Giemsa solution. For evaluation of female fertility for 15 weeks, an 8- or 24-week-old wild-type or $AR^{-/-}$ female was mated with a wild-type fertile male, replaced every 2 weeks with the other fertile male. Cages were monitored daily and for an additional 23 days, and the presence of seminal plugs and number of litters were recorded.

RNA Extraction and Quantitative Competitive RT-PCR. Total ovarian RNA was extracted by using TRIzol (Invitrogen) (16). Oligo-dT-primed cDNA was synthesized from 1 μg of ovarian RNA by using SuperScript reverse transcriptase (Gibco BRL, Gaithersburg, MD) in a 20-μl reaction volume, 1 μl of which was then diluted serially (2- to 128-fold) and used to PCR-amplify an internal control gene, cycA, to allow concentration estimation.
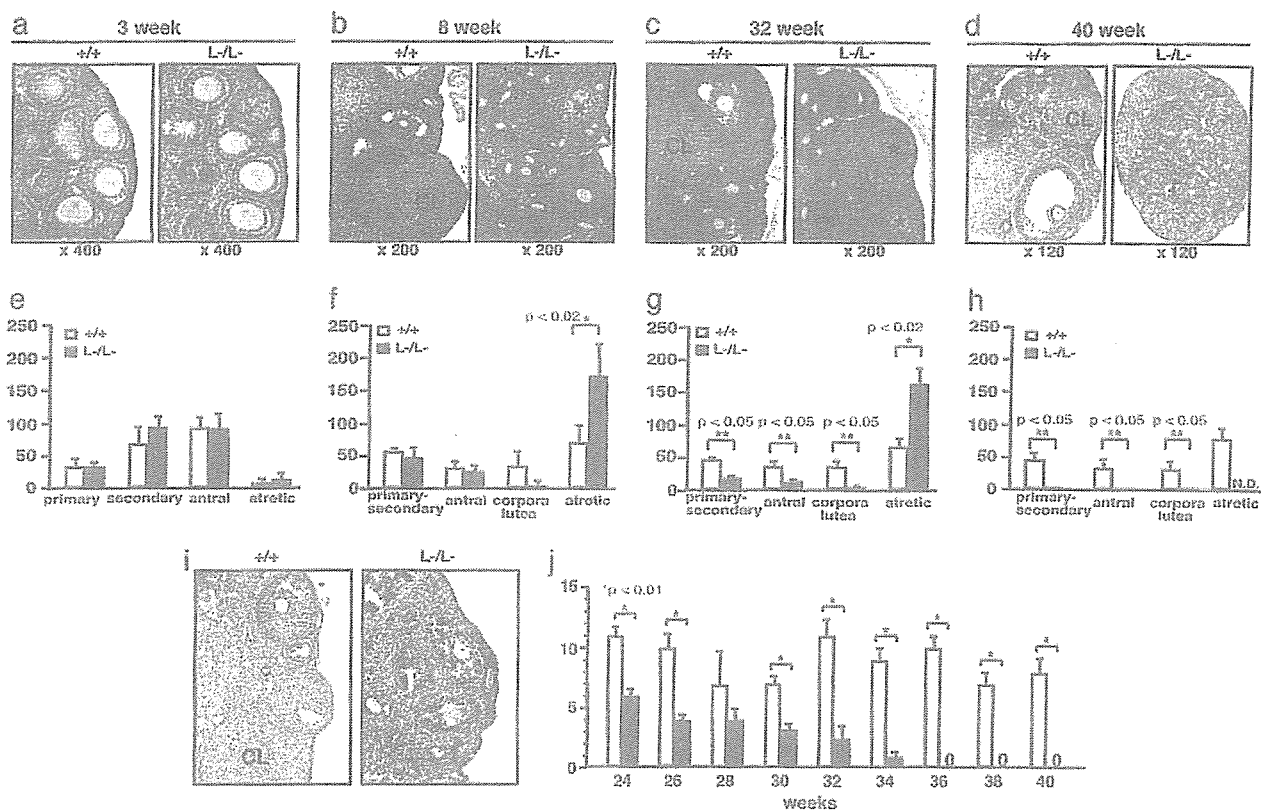
Fig. 2. POF in AR$^{-/-}$ female mice. (a-d) Histology of AR$^{+/+}$ and AR$^{-/-}$ ovaries at 3 weeks, 8 weeks, 32 weeks, and 40 weeks of age. All sections were stained with hematoxylin and eosin. An asterisk marks the atretic follicle. CL, corpus luteum. (e-h) Relative follicle counts at 3 weeks (e), 8 weeks (f), 32 weeks (g), and 40 weeks (h) of age. Numbers represent total counts of every fifth section from serially sectioned ovaries (n = 4 animals per genotype). (i) Immunohistochemical study for activated, cleaved caspase-3 revealed increased positive cells (apoptotic cells) in AR$^{-/-}$ ovaries. Sections were counterstained with hematoxylin. An asterisk marks the caspase-3-positive cell. CL, corpus luteum. (j) Age-dependent reduction in the number of pups per litter in AR$^{-/-}$ female mice. A continuous breeding assay was started at 24 weeks of age (n = 6–10 animals per genotype). For all panels, data are shown as mean ± SEM and were analyzed by using Student's t test.

Primers were designed from cDNA sequences of *Kitl* (M57647; nucleotides 1099–1751), *Gdf9* (NM008110; nucleotides 720-1532), *Bmp15* (NM009757; nucleotides 146–973), *Ers2* (NM010157; nucleotides 1139-1921), *Pgr* (NM008829; nucleotides 1587–2425), *Cyp11a1* (NM019779; nucleotides 761-1697), *Cyp17a1* (M64863; nucleotides 522–932), *Cyp19* (D00659; nucleotides 699-1049), *Fshr* (AF095642; nucleotides 625-1427), *Lhr* (M81310; nucleotides 592-1331), *Ptgs2* (AF338730; nucleotides 3–605), and *Ccnd2* (NM009829; nucleotides 150-1065) and chosen from different exons to avoid amplification from genomic DNA.

GeneChip Analysis. Ovaries were isolated and stabilized in RNA-later RNA Stabilization Reagent (Ambion, Austin, TX) before RNA purification (17). Total RNA was purified by using an RNeasy mini kit (Qiagen, Valencia, CA) according to the manufacturer's instructions. First-strand cDNA was synthesized from 5 μg of RNA by using 200 units of SuperScript II reverse transcriptase (Invitrogen, Carlsbad, CA), 100 pmol T7-(dT)$_{24}$ primer [5′-GGCCAGTGAATTGTAATACGACTCAC-TATAGGGAGGCGG-(dT)$_{24}$-3′], 1× first-strand buffer, and 0.5 mM dNTPs at 42°C for 1 h. Second-strand synthesis was performed by incubating first-strand cDNA with 10 units of *Escherichia coli* ligase (Invitrogen), 40 units of DNA polymerase I (Invitrogen), 2 units of RNase H (Invitrogen), 1× reaction buffer, and 0.2 mM dNTPs at 16°C for 2 h, followed by 10 units of T4 DNA polymerase (Invitrogen) and incubation for another

5 min at 16°C. Double-stranded cDNA was purified by using GeneChip Sample Cleanup Module (Affymetrix, Santa Clara, CA) according to the manufacturer's instructions and labeled by *in vitro* transcription by using a BioArray HighYield RNA transcript labeling kit (Enzo Diagnostics, Farmingdale, NY). Briefly, dsDNA was mixed with 1× HY reaction buffer, 1× biotin-labeled ribonucleotides (NTPs with Bio-UTP and Bio-CTP), 1× DTT, 1× RNase inhibitor mix, and 1× T7 RNA polymerase and incubated at 37°C for 4 h. Labeled cRNA was then purified by using GeneChip Sample Cleanup Module and fragmented in 1× fragmentation buffer at 94°C for 35 min. For hybridization to the GeneChip Mouse Expression Array 430A or 430B or Mouse Genome 430 2.0 Array (Affymetrix), 15 μg of fragmented cRNA probe was incubated with 50 pM control oligonucleotide B2, 1× eukaryotic hybridization control, 0.1 mg/ml herring sperm DNA, 0.5 mg/ml acetylated BSA, and 1× hybridization buffer in a 45°C rotisserie oven for 16 h. Washing and staining were performed by using a GeneChip Fluidic Station (Affymetrix) according to the manufacturer's protocol. Phycoerythrin-stained arrays were scanned as digital image files and analyzed with GENECHIP OPERATING SOFTWARE (Affymetrix) (17).

Luciferase Assay. The *Kitl* promoter region (−2866 to −1 bp) was inserted into the pGL3-basic vector (Promega) for assay using the Luciferase Assay System (Promega) (14, 16). Cells at 40–50% confluence were transfected with a reference pRL-CMV
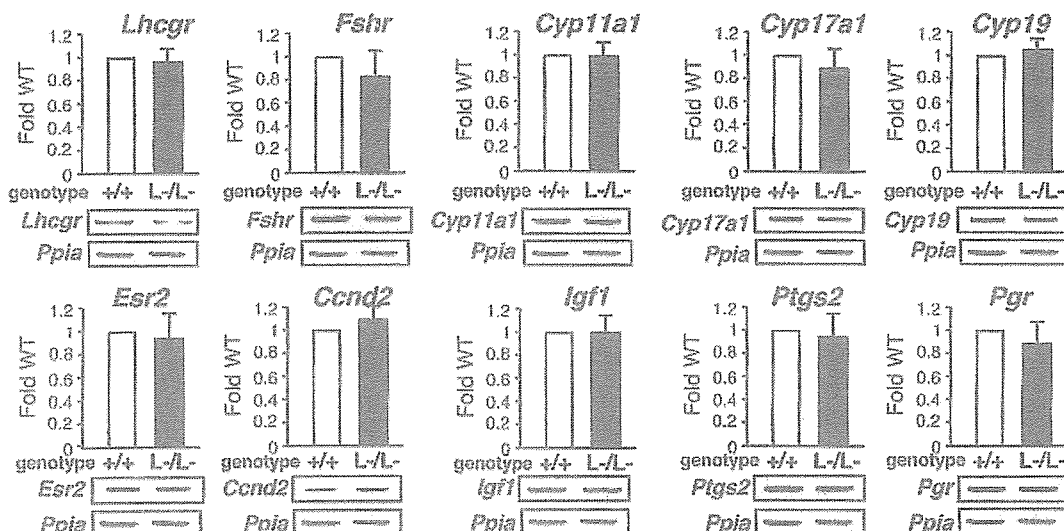
Fig. 3. No significant alterations in mRNA levels of several major regulators in folliculogenesis. Shown is semiquantitative RT-PCR of LH receptor (*Lhr*), FSH receptor (*Fshr*), p450 side chain cleavage enzyme (*Cyp11a1*), 17-α-hydroxylase (*Cyp17a1*), Aromatase (*Cyp19*), estrogen receptor-β (*Esr2*), cyclin D2 (*Ccnd2*), insulin-like growth factor 1 (*Igf1*), cyclooxygenase 2 (*Ptgs2*), or progesterone receptor (*Pgr*) gene expression in $AR^{+/+}$ and $AR^{-/-}$ ovaries. Results shown were representative (using one ovary per genotype in each experiment) of five independent experiments.

plasmid (Promega) using Lipofectamine reagent (GIBCO/BRL, Grand Island, NY) to normalize transfection. Results shown are representative of five independent experiments.

Results and Discussion

Subfertility of $AR^{-/-}$ Female Mice at 8 Weeks of Age.

The *Ar* gene located on the X chromosome was disrupted in mice by using the Cre/Lox P system (6) (Fig. 1 *a–c*). Female $AR^{-/-}$ mice showed normal growth compared with the wild-type littermates (Fig. 1*d*), with no detectable bone loss (Fig. 1*e*) or obesity common for male $AR^{-/-}$ mice (8, 9). Young (8-week-old) $AR^{-/-}$ females appeared indistinguishable from the wild-type littermates, displayed normal sexual behavior (7), and produced the first offspring of normal body size at the expected age. Macroscopic appearance of their reproductive organs, including uteri, oviducts, and ovaries, also appeared normal (Fig. 1*f*). Histological analysis showed no significant abnormality in the uterus or pituitary (Fig. 1*e*), whereas mammary ductal branching and elongation were substantially reduced, as revealed by whole-mount analysis (Fig. 1*h*). Serum levels of 17β-estradiol, progesterone, testosterone, luteinizing hormone, and follicle-stimulating hormone were also within normal range in 8-week-old mutant females at the proestrus stage (Fig. 1*g*), suggesting that the two-cell two-gonadotrophin system in female reproductive and endocrine organs (18) was intact in $AR^{-/-}$ mice at 8 weeks of age. The most obvious early sign of abnormal reproductive function in the $AR^{-/-}$ females was that their average numbers of pups per litter were only about half of those of the wild-type littermates, ($AR^{+/-}$, 8.3 ± 0.4 pups per litter; $AR^{-/-}$, 4.5 ± 0.5 pups per litter) (Fig. 1*i*).

$AR^{-/-}$ Female Mice Developed POF Phenotypes.

Histological analysis of 8-week-old $AR^{-/-}$ ovaries clearly showed that numbers of atretic follicles were significantly increased, with decreased numbers of corpora lutea (Fig. 2 *b* and *f*). This finding suggests that the reduced pup numbers were due to impaired folliculogenesis in AR-deficient ovaries. Indeed, AR protein expression was readily detectable in the wild-type 8-week-old ovaries (Fig. 1*j*), with AR expressed at the highest levels in growing follicle granulosa cells at all developmental stages and at relatively low

levels in corpora lutea. Thus, AR appears to play a regulatory role in granulosa cells during their maturation to the luteal phase.

To investigate this possibility, we examined the ovarian phenotype of female $AR^{-/-}$ mice at different ages. At 3 weeks, ovaries contain various stages of follicles, including primary, secondary, and antral follicles in wild-type animals (Fig. 2*a*) (19). In $AR^{-/-}$ ovaries at 3 weeks of age, the folliculogenesis appeared to be unaltered, with normal numbers and localization of primary and secondary follicles (Fig. 2 *a* and *e*). However, degenerated folliculogenesis became evident with further aging. Although follicles and corpora lutea at all developmental stages were still present, corpora lutea numbers were clearly reduced in 8-week-old $AR^{-/-}$ mutants (Fig. 2 *b* and *f*), similar to that observed in another mouse line (20). Expected apoptosis was seen in atretic follicles by activated caspase-3 immunohistochemistry assays (Fig. 2*i*). But, by 32 weeks of age, defects in folliculogenesis in $AR^{-/-}$ ovaries became profound, with fewer follicles observed and increased atretic follicles (Fig. 2 *c* and *g*), and >40% (5 of 12 mice) of the $AR^{-/-}$ females were already infertile. By 40 weeks, all $AR^{-/-}$ females became infertile, with no follicles remaining (Fig. 2 *d* and *h*); at the same age, $AR^{+/+}$ females were fertile and had normal follicle numbers. Consistent with progressive deficiency in folliculogenesis, the pup number per litter steadily decreased in aging $AR^{-/-}$ females (Fig. 2*i*). These data indicate that AR plays an important physiological role at the preluteal phase of folliculogenesis.

Alteration in Gene Expressions of Several Major Regulators Involved in the Oocyte–Granulosa Cell Regulatory Loop.

To explore the molecular basis underlying the impaired folliculogenesis in $AR^{-/-}$ ovaries, we analyzed expression of several major known regulators and markers of folliculogenesis (21–23). Surprisingly, no significant alterations in mRNA levels of LH receptor (*Lhr*), FSH receptor (*Fshr*), p450 side chain cleavage enzyme (*Cyp11a1*), 17-α-hydroxylase (*Cyp17a1*), aromatase (*Cyp19*), estrogen receptor-β (*Esr2*), cyclin D2 (*Ccnd2*), or insulin-like growth factor 1 (*Igf1*) of 8-week-old $AR^{-/-}$ ovaries at the proestrus stage, and further cyclooxygenase 2 (*Ptgs2*) or progesterone receptor (*Pgr*) at the estrus stage, were detected by
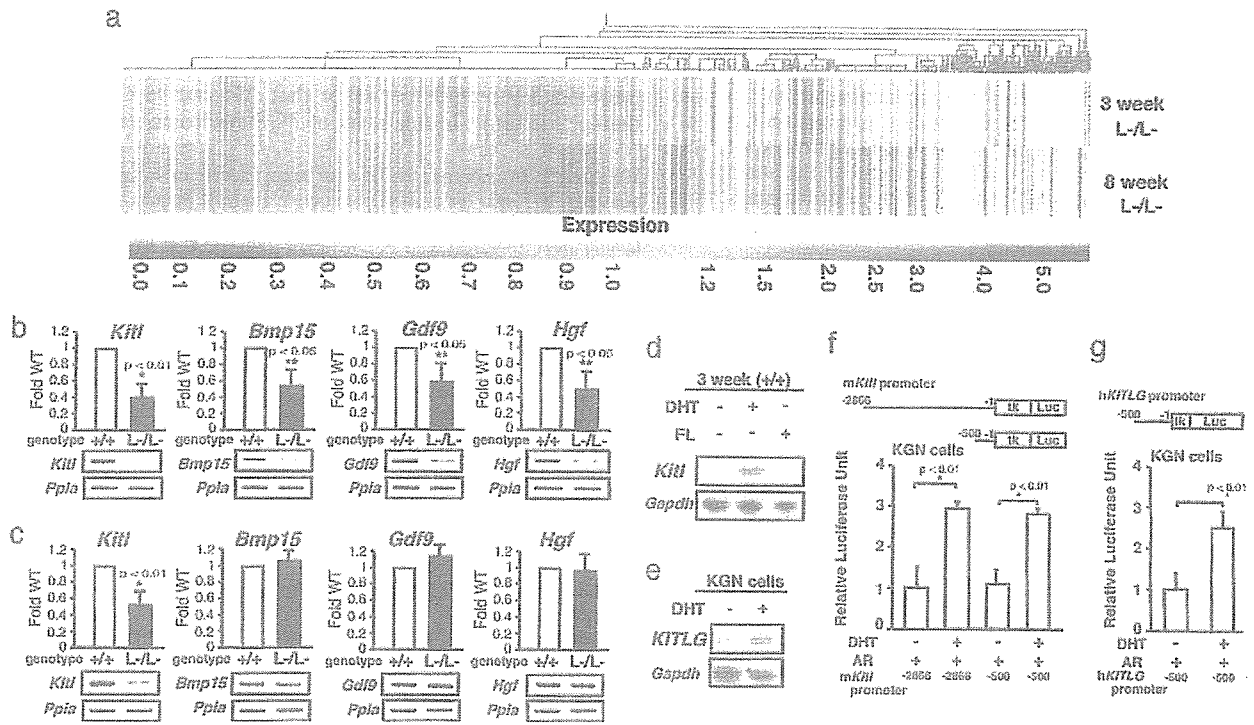
PHYSIOLOGY

Fig. 4. Genome-wide microarray analysis and semiquantitative RT-PCR revealed that expression of the oocyte-granulosa cell regulator loop was down-regulated in $AR^{-/-}$ ovaries. (a) Microarray analysis of $AR^{-/-}$ compared with $AR^{+/+}$ ovaries at 3 and 8 weeks of age. Data obtained from microarray analysis as described in Materials and Methods were used to generate a cluster analysis. Each vertical line represents a single gene. The ratios of gene expression levels in $AR^{-/-}$ ovaries compared with wild type are presented. (b and c) Semiquantitative RT-PCR analysis of AR-regulated genes identified from the microarray study. Results shown are representative (using one ovary per genotype in each experiment) of five independent experiments. Data are shown as mean ± SEM and were analyzed by using Student's t test. (d) Comparison of Kitl gene expression by Northern blot analysis among placebo-, DHT-, and flutamide (FL)-treated $AR^{+/+}$ mouse ovaries. (e) Induction of KITLG gene expression by DHT treatment in KGN cells. (f and g) Androgen responsiveness in the mouse and human kit ligand promoters by a luciferase assay performed by using KGN cells. Data are shown as mean ± SEM and were analyzed by using Student's t test.

semiquantitative RT-PCR analysis (Fig. 3). Genome-wide microarray analysis (17) of RNA from 8-week-old $AR^{-/-}$ ovaries at the proestrus stage has been undertaken to identify AR-regulated genes. In comparison with $AR^{+/+}$ ovaries, expressions of 772 genes were down-regulated, whereas 351 genes were up-regulated in $AR^{-/-}$ ovaries (Fig. 4a; see also Tables 1 and 2, which are published as supporting information on the PNAS web site). Several genes known to be involved in the oocyte–granulosa cell regulatory loop (24) were identified as candidate AR target genes, including KIT ligand (Kitl) (25), morphogenetic protein 15 (Bmp15) (26), growth differentiation factor-9 (Gdf9) (27), and hepatocyte growth factor (Hgf) (28). Impaired folliculogenesis had been reported in mice deficient in each of these three regulators (26, 27, 29). To validate the microarray data, we performed semiquantitative RT-PCR analysis of 8-week-old $AR^{-/-}$ ovary RNA and confirmed that expression of these factors was down-regulated (Fig. 4b). To identify a regulator downstream of the AR signaling at an earlier stage of folliculogenesis, 3-week-old $AR^{-/-}$ ovaries that, as pointed out earlier, display no apparent phenotypic abnormality were examined. Fewer genes had altered expression levels (519 genes up-regulated; 326 genes down-regulated) (Fig. 4a; see also Tables 3 and 4, which are published as supporting information on the PNAS web site), and, of the four regulators tested by RT-PCR, only Kitl was found to be down-regulated at this age (Fig. 4c). Because Kitl is a granulosa cell-derived factor and stimulates oocyte growth and maturation (29–31), down-regulation of the Kitl expression in 3-week-old or even younger $AR^{-/-}$ ovaries may trigger impairment in folliculogenesis at a

later age. To test for possible Kitl gene regulation by AR, 3-week-old wild-type females were treated with 5α-dihydrotestosterone (DHT). At 4 h after hormone injection, a clear induction of Kitl expression was observed in the ovaries, whereas a known antiandrogen flutamide attenuated the induction by DHT (Fig. 4d). The induction of endogenous human kit ligand (KITLG) gene by DHT was also observed in human granulosa-like tumor cells (KGN) in culture (Fig. 4e). Furthermore, androgen-induced transactivation of mouse and human kit ligand promoters (32) was observed by a luciferase reporter assay (33) in KGN (Fig. 4 f and g), 293T, and HeLa (data not shown) cells. However, no response to DHT was detected in the similar assay using promoters of the Bmp15, Gdf9, and Hgf genes (data not shown). Thus, we have shown that, in a regulatory cascade controlling folliculogenesis, Kitl represents a direct downstream target of androgen signaling.

As an upstream regulator, AR may also be indirectly involved in control of expression of other genes critical for folliculogenesis, because an age-dependent down-regulation of Bmp15, Gdf9, and Hgf gene expression was also observed in $AR^{-/-}$ ovaries. Bmp15 and Gdf9 are oocyte-derived factors that promote the development of surrounding granulosa cells in growing follicles (34, 35), whereas Hgf is secreted by theca cells and acts as a granulosa cell growth factor (36). Down-regulation of these factors, presumably due to decreased Kitl expression, may lead to impaired bidirectional communication between oocyte and granulosa cells (24) and, eventually, to early termination of folliculogenesis, as in POF syndrome.

Thus, we have identified AR as a novel regulator of follicu-

Shiina et al.

logenesis that apparently acts in the regulatory cascade upstream of the major factors controlling ovarian function, confirming the previous findings of the AR expression in granulose cells of growing follicles (3). Although not immediately relevant to the ovarian physiology, abnormal development of the mammary glands observed in our AR-deficient mice adds further strong evidence of an essential role of the AR not only in male, but also in female, reproductive function.

With increasing age of the first childbirth by women in the modern society, POF syndrome has become an important social and medical problem. Our findings suggest that POF syndrome may be caused by an impairment in androgen signaling and that X chromosomal mutations affecting the *AR* gene function may

play a key role in hereditary POF. From clinical perspective, the present study provides evidence that AR can be a beneficial therapeutic target in treatment of POF syndrome patients.

1. Laml, T., Preyer, O., Umek, W., Hengstschlager, M. & Hanzal, H. (2002) *Hum. Reprod. Update* 8, 483–491.
2. Davison, R. M., Davis, C. J. & Conway, G. S. (1999) *Clin. Endocrinol. (Oxford)* 51, 673–679.
3. Tetsuka, M., Whitelaw, P. F., Bremner, W. J., Millar, M. R., Smyth, C. D. & Hillier, S. G. (1995) *J. Endocrinol.* 145, 535–543.
4. Ehrmann, D. A., Barnes, R. B. & Rosenfield, R. L. (1995) *Endocr. Rev.* 16, 322–353.
5. Norman, R. J. (2002) *Mol. Cell. Endocrinol.* 191, 113–119.
6. Kato, S. (2002) *Clin. Pediatr. Endocrinol.* 11, 1–7.
7. Sato, T., Matsumoto, T., Kawano, H., Watanabe, T., Uematsu, Y., Sekine, K., Fukuda, T., Aihara, K., Krust, A., Yamada, T., et al. (2004) *Proc. Natl. Acad. Sci. USA* 101, 1673–1678.
8. Sato, T., Matsumoto, T., Yamada, T., Watanabe, T., Kawano, H. & Kato, S. (2003) *Biochem. Biophys. Res. Commun.* 300, 167–171.
9. Kawano, H., Sato, T., Yamada, T., Matsumoto, T., Sekine, K., Watanabe, T., Nakamura, T., Fukuda, T., Yoshimura, K., Yoshizawa, T., et al. (2003) *Proc. Natl. Acad. Sci. USA* 100, 9416–9421.
10. Li, M., Indra, A. K., Warot, X., Brocard, J., Messaddeq, N., Kato, S., Metzger, D. & Chambon, P. (2000) *Nature* 407, 633–636.
11. Sekine, K., Ohuchi, H., Fujiwara, M., Yamasaki, M., Yoshizawa, T., Sato, T., Yagishita, N., Matsui, D., Koga, Y., Itoh, N. & Kato, S. (1999) *Nat. Genet.* 21, 138–141.
12. Yoshizawa, T., Handa, Y., Uematsu, Y., Takeda, S., Sekine, K., Yoshihara, Y., Kawakami, T., Arioka, K., Sato, H., Uchiyama, Y., et al. (1997) *Nat. Genet.* 16, 391–396.
13. Gubbay, J., Collignon, J., Koopman, P., Capel, B., Economou, A., Munsterberg, A., Vivian, N., Goodfellow, P. & Lovell-Badge, R. (1990) *Nature* 346, 245–250.
14. Yanagisawa, J., Yanagi, Y., Masuhiro, Y., Suzawa, M., Watanabe, M., Kashiwagi, K., Toriyabe, T., Kawabata, M., Miyazono, K. & Kato, S. (1999) *Science* 283, 1317–1321.
15. Britt, K. L., Indra, A. E., Cox, V. A., Dyson, M., Wreford, N. G., Jones, M. E., Simpson, E. R. & Findlay, J. K. (2000) *Endocrinology* 141, 2614–2623.
16. Ohtake, F., Takeyama, K., Matsumoto, T., Kitagawa, H., Yamamoto, Y., Nohara, K., Tohyama, C., Krust, A., Mimura, J., Chambon, P., et al. (2003) *Nature* 423, 545–550.
17. Fujimoto, N., Igarashi, K., Kanno, J., Honda, H. & Inoue, T. (2004) *J. Steroid Biochem. Mol. Biol.* 91, 121–129.
18. Couse, J. F. & Korach, K. S. (1999) *Endocr. Rev.* 20, 358–417.
19. Elvin, J. A. & Matzuk, M. M. (1998) *Rev. Reprod.* 3, 183–195.
20. Hu, Y. C., Wang, P. H., Yeh, S., Wang, R. S., Xie, C., Xu, Q., Zhou, X., Chao, H. T., Tsai, M. Y. & Chang, C. (2004) *Proc. Natl. Acad. Sci. USA* 101, 11209–11214.
21. Elvin, J. A., Yan, C., Wang, P., Nishimori, K. & Matzuk, M. M. (1999) *Mol. Endocrinol.* 13, 1018–1034.
22. Zhou, J., Kumar, T. R., Matzuk, M. M. & Bondy, C. (1997) *Mol. Endocrinol.* 11, 1924–1933.
23. Burns, K. H., Yan, C., Kumar, T. R. & Matzuk, M. M. (2001) *Endocrinology* 142, 2742–2751.
24. Matzuk, M. M., Burns, K. H., Viveiros, M. M. & Eppig, J. J. (2002) *Science* 296, 2178–2180.
25. Joyce, I. M., Pendola, F. L., Wigglesworth, K. & Eppig, J. J. (1999) *Dev. Biol.* 214, 342–353.
26. Yan, C., Wang, P., DeMayo, J., DeMayo, F. J., Elvin, J. A., Carino, C., Prasad, S. V., Skinner, S. S., Dunbar, B. S., Dube, J. L., et al. (2001) *Mol. Endocrinol.* 15, 854–866.
27. Dong, J., Albertini, D. F., Nishimori, K., Kumar, T. R., Lu, N. & Matzuk, M. M. (1996) *Nature* 383, 531–535.
28. Parrott, J. A., Vigne, J. L., Chu, B. Z. & Skinner, M. K. (1994) *Endocrinology* 135, 569–575.
29. Driancourt, M. A., Reynaud, K., Cortvrindt, R. & Smitz, J. (2000) *Rev. Reprod.* 5, 143–152.
30. Huang, E. J., Manova, K., Packer, A. I., Sanchez, S., Bachvarova, R. F. & Besmer, P. (1993) *Dev. Biol.* 157, 100–109.
31. Packer, A. I., Hsu, Y. C., Besmer, P. & Bachvarova, R. F. (1994) *Dev. Biol.* 161, 194–205.
32. Grimaldi, P., Capolunghi, F., Geremia, R. & Rossi, P. (2003) *Biol. Reprod.* 69, 1979–1988.
33. Kitagawa, H., Fujiki, R., Yoshimura, K., Mezaki, Y., Uematsu, Y., Matsui, D., Ogawa, S., Unno, K., Okubo, M., Tokita, A., et al. (2003) *Cell* 113, 905–917.
34. Otsuka, F. & Shimasaki, S. (2002) *Proc. Natl. Acad. Sci. USA* 99, 8060–8065.
35. Joyce, I. M., Clark, A. T., Pendola, F. L. & Eppig, J. J. (2000) *Biol. Reprod.* 63, 1669–1675.
36. Parrott, J. A. & Skinner, M. K. (1998) *Endocrinology* 139, 2240–2245.

BMC Genomics

Methodology article

"Per cell" normalization method for mRNA measurement by quantitative PCR and microarrays

Jun Kanno*[†1], Ken-ichi Aisaki[†1], Katsuhide Igarashi[1], Noriyuki Nakatsu[1], Atsushi Ono[1], Yukio Kodama[1] and Taku Nagao[2]

Address: [1]Division of Cellular and Molecular Toxicology, National Institute of Health Sciences, 1-18-1, Kamiyoga, Setagaya-ku, Tokyo 158-8501, Japan and [2]President, National Institute of Health Sciences, 1-18-1, Kamiyoga, Setagaya-ku, Tokyo 158-8501, Japan

Email: Jun Kanno* - kanno@nihs.go.jp; Ken-ichi Aisaki - aisaki@nihs.go.jp; Katsuhide Igarashi - igarashi@nihs.go.jp; Noriyuki Nakatsu - n-nakatsu@nihs.go.jp; Atsushi Ono - Atsushi@nibio.go.jp; Yukio Kodama - kodama@nihs.go.jp; Taku Nagao - nagao@nihs.go.jp

* Corresponding author   †Equal contributors

Abstract

Background: Transcriptome data from quantitative PCR (Q-PCR) and DNA microarrays are typically obtained from a fixed amount of RNA collected per sample. Therefore, variations in tissue cellularity and RNA yield across samples in an experimental series compromise accurate determination of the absolute level of each mRNA species per cell in any sample. Since mRNAs are copied from genomic DNA, the simplest way to express mRNA level would be as copy number per template DNA, or more practically, as copy number per cell.

Results: Here we report a method (designated the "Percellome" method) for normalizing the expression of mRNA values in biological samples. It provides a "per cell" readout in mRNA copy number and is applicable to both quantitative PCR (Q-PCR) and DNA microarray studies. The genomic DNA content of each sample homogenate was measured from a small aliquot to derive the number of cells in the sample. A cocktail of five external spike RNAs admixed in a dose-graded manner (dose-graded spike cocktail; GSC) was prepared and added to each homogenate in proportion to its DNA content. In this way, the spike mRNAs represented absolute copy numbers per cell in the sample. The signals from the five spike mRNAs were used as a dose-response standard curve for each sample, enabling us to convert all the signals measured to copy numbers per cell in an expression profile-independent manner. A series of samples was measured by Q-PCR and Affymetrix GeneChip microarrays using this Percellome method, and the results showed up to 90 % concordance.

Conclusion: Percellome data can be compared directly among samples and among different studies, and between different platforms, without further normalization. Therefore, "percellome" normalization can serve as a standard method for exchanging and comparing data across different platforms and among different laboratories.

Background

Normalization of gene expression data between different samples generated in the same laboratory using a single platform, and/or generated in different geographical